84
93

RANDOM VIBRATIONS OF BLADED-DISK ASSEMBLY UNDER CYCLOSTATIONARY EXCITATION

by

Sveinn V. Olafsson

Thesis submitted to the Faculty of the
Virginia Polytechnic Institute and State University
in partial fulfillment of the requirements for the degree of

MASTER OF SCIENCE

in

Aerospace Engineering

APPROVED:

Dr. Efstratios Nikolaidis, Chairman

Dr. Rakesh Kapania

Dr. Eric Johnson

Dr. Roger L. Simpson

June 1988
Blacksburg, Virginia

Random Vibrations of Bladed-Disk Assemblies
under Cyclostationary Excitation

by

Sveinn V. Olafsson

Dr. E. Nikolaidis, Chairman
Aerospace Engineering

(ABSTRACT)

Random vibration of a bladed-disk assembly is studied. A stochastic model for the excitation is developed. A unique feature of this model is the statistical periodicity of the blade forces called cyclostationary. A random process is called wide sense cyclostationary and its statistics are periodic in time. Factors like the turbulent nature of the flow around the blades, the variability in their geometry, and their nonuniform deterioration contribute to the uncertainty in the excitation. In periodic structures, like the bladed-disk assembly, small variation in the blade excitation may lead to high variability in the response.

The model developed includes both random and deterministic excitation. A comparison of the responses due to the random and the deterministic part shows the significance of taking into account the variability in the blade forces.

Therefore the assumption that the blade forces are all equal, used by all methods for vibration analysis of bladed disk assemblies, may lead to erroneous estimates of their response, reliability and expected life.

It is shown that the response is a cyclostationary process. Therefore the cyclostationary property is preserved from the input to

the output. Furthermore the frequency of the second moment of the response is equal to two times the frequency of the excitation.

Acknowledgements

I would like to thank my advisor, Dr. Efstratios Nikolaidis, for his continued interest and enthusiasm in the progress of my research and studies and Virginia Polytechnic Institute and State University. I would also like to thank my committee members, Dr. Rakesh Kapania, Dr. Eric Johnson, and Dr. Roger L. Simpson for the time they have spent reviewing this work as well as the willingness of many other professors at VPI&SU to offer suggestions for my progress. I am further thankful of Dr. Joseph A. Schetz for his support of my studies and research.

My family in Iceland also gets warm thanks for their encouragement and support during my studies and always when needed.

Table of Contents

List of Tables

List of Figures

Nomenclature

a	deterministic velocity amplitude
C	damping constant
C_1, C_3	time constants
C_2, C_4	spatial constants
C_L	coefficient of lift
d_{ij}	elements in dynamic matrix of the bladed-disk assembly
$D(\omega)$	dynamic matrix
F_{1_k}	mean lift force
F_L	lift force
F_n	n^{th} blade force
f_n	amplitude of the n^{th} blade force
$H_i(\omega)$	i^{th} element of transfer matrix/vector
K_i	the i^{th} stiffness
m_i	the i^{th} mass
N	number of blades
$P_{1_k}(t)$	periodic function, nonzero mean
$\tilde{P}_{1_k}(t)$	periodic function, zero mean
$P_{2_k}(t)$	periodic function, zero mean
$R_{F_pF_q}$	cross-correlation function, of forces F_p and F_q
$R_r(t+\tau,t)$	autocorrelation function, response
r	radius
S	number of stators

$S_{\alpha_i \alpha_k}(\omega)$	velocity spectrum
V_{i_k}	instantaneous inflow velocity from k^{th} stator
$\bar{V}_i$	mean inflow velocity
$V^*_{i_k}$	perpendicular velocity
V_{rel_i}	instantaneous relative velocity
V_X	velocity parallel to an airfoil
V_Y	velocity perpendicular to an airfoil
V_∞	free stream velocity
X_{eq}	displacement due to forces with equal amplitude
X_{max}	maximum displacement
X_i	displacement of the i^{th} blade

Greek:

α	angle of attack
$\alpha_k(t)$	random part of parallel inflow velocity
α_1	mean angle of attack
β	zero lift angle
β_1	mean relative velocity flow angle
δ	rotor blade angle
$\Delta_{F_p F_q}$	double Fourier transform of the cross-correlation function of forces F_p and F_q
ΔF_{i_k}	derivative of the blade force with respect to the inflow velocity under mean conditions
$\Delta F^*_{i_k}$	derivative of the blade force with respect to the perpendicular velocity under mean conditions
$\gamma_k(t)$	random part of perpendicular inflow velocity
ϕ_i	phase angle
ρ	density of air
μ_F	mean force
μ_X	mean displacement
ω	angular velocity
ω_o	natural frequency
σ_α	standard deviation of parallel inflow velocity
σ_γ	standard deviation of perpendicular inflow velocity
σ_F	standard deviation of force F
σ_X	standard deviation of displacement X

θ_1	stator blade angle
τ	time difference

Chapter 1. Introduction

1.1 Introduction

Most modern aircrafts are powered by some form of a gas turbine engine. Introduction of large scale gas turbine propulsion systems started in the military sector in the 1950s and in commercial aircrafts in 1960s. Since then the cost effectiveness, performance and efficiency of these engines have improved dramatically.

Safety is a factor of primary concern in any aircraft design. The aircraft must as a whole be safe enough to fly. History of accidents shows that the engine is the most critical part of any aircraft.

The first jet engines were not very reliable; they ran only for few hours often breaking within that period of time. Gradually gas turbine design and manufacturing was improved. Today these engines have become so safe that people are talking about having no limitations on twin-engine planes, like Boeing 767s and Airbus A310s, flying over water. This would not be under discussion if it were not far more reliable and sophisticated methods for design and analysis.

A modern turbofan engine consists of the following major components [OATE 84],[KERR 77]: The inlet manifold, the fan, the compressor and the turbine. In the following we briefly describe the base operation principles of a aircraft gas turbine, such as the one in Figure 1. First the air passes through the inlet manifold, whose purpose is to slow down the air and thereby increase its pressure before it goes through the fan. The fan is driven by the turbine and it acts like a propeller i.e. it produces majority of the total thrust

generated by the engine. After passing through the fan the air either goes out to the atmosphere through a fan-nozzle or it goes into the compressor. In the compressor, that is the third major component, the air is compressed up to an efficient burning pressure for the burner or the combustion chamber, that is next in the row. Fuel is now injected and the air-fuel mixture is burned. This high pressured hot gas enters the turbine. Here the pressure decreases and before the exhaust gas is let into the atmosphere it goes through a nozzle to accelerate it. Since the velocity of the air coming out of the engine is higher than the inlet velocity a net thrust is created.

This operational principle sounds simple, but a number of problems that are very complex are involved in analysis and design of gas turbines. The understanding of sophisticated engineering systems including principles of fluid and solid mechanics, chemistry, automatic control etc. is necessary in both the analysis and design tasks.

The problem of designing the compressor and/or the turbine is of great importance. These components must be able to withstand great stresses at a very high temperature. Therefore it is very important to be able to accurately predict the vibrations of these bladed-disk assemblies. The critical nature of the problem becomes apparent when one notes that there can be as many as thousand blades in one engine of advanced design. Therefore, the determination of dynamic characteristics of the blades becomes important in the design phase.

State-of-the-art methods on the analysis of bladed-disk assemblies, assume that the blade forces are deterministic and that

all of them have the same amplitude. In reality the blade forces change in time but also vary from blade to blade in a random fashion. This variability is due to the random nature of the turbulent flow around blades, imperfections in the geometry of each blade and their nonuniform deterioration. In Figure 2 we can see how the mean value of the instantaneous flow velocity varies. This goes up between stator blades and down in the wakes behind them. On the same figure we can also see the root mean square value (RMS) of the instantaneous flow velocity. The root mean square serves as a good measure of the turbulence intensity. It takes its highest value in the wakes behind the stator blades and lowest between them, that is opposite to the way that the mean velocity changes. These variations in the flow velocity affect the incident angle that each rotor blade sees as shown in Figure 3. Consequently the blade force can vary significantly. A sample path of a blade force is drawn in Figure 4. If we assume that the blade forces are functions of the flow velocity only we conclude that they will vary in the same manner.

We will study the deterministic case separately since it is a function of the mean flow velocity only. The random part is due to the turbulent variation of the velocity. A unique feature of the blade forces is their statistical periodicity called cyclostationary. A random process is called wide sense cyclostationary if its statistics are periodic in time. Indeed statistical quantities like the mean value and the RMS of the forces are not constant but they vary periodically in time. The nonstationary character of the blade forces makes conventional approaches for evaluating the response of

linear systems under stationary excitation inappropriate for solving our problem. A new approach originally developed in statistical communication theory and adapted by Nikolaidis for the analysis of linear mechanical systems [NIKO 87] under cyclostationary excitation is applied, to evaluate the response of the blades. The analysis performed in the following sections shows that the cyclostationary nature is preserved from the input (forces) to the output (response).

Ignoring the variability in the blade forces may lead to erroneous estimates of vibratory stresses and deflections of the blades. These estimates may lie on the nonconservative side.

1.2 Objectives

As it was mentioned in section 1.1, state-of-the-art methods on the analysis of bladed-disk assemblies, assume that the blade forces are deterministic and that all of them have the same amplitude. In periodic structures like the bladed-disk assembly, small variabilities in the blade excitation may lead to high variability in the response.

The scope of this study is to demonstrate the importance of randomness in blade excitation and develop a probabilistic method for analyzing their response that takes into account the variability in blade forces.

The objectives of this thesis are:

- To develop a model for the excitation that takes into account the cyclostationary property of the blade forces.

- Show that in periodic structures, like the bladed-disk assembly, small variabilities in the blade excitation may lead to high variability in the response.
- Develop an approach for calculating the statistics of the response of the blades from those of the exciting forces.

It is shown that the response is a cyclostationary process. Therefore the cyclostationary property is preserved from the input to the output. The solution of the problem is based on the following assumptions:

(i) For the nonresonant case, the displacement of the blades is negligible compared with the displacement under resonant conditions.

(ii) In case of resonance, the nonresonant harmonics of the excitation can be neglected in the evaluation of the displacement.

The results of this research will increase the understanding of the topic of vibrations of bladed-disk assemblies, and promote the design of more efficient and safer turbomachinery components.

1.3. Literature Review

The last decade has been active for research in the area of vibrations of propeller, windmill and turbine blades reflecting an increased awareness of the complexity and importance of the topic. Most of the research in this area has been based on the assumption that parameters such as geometrical properties of the bladed-disk assembly, damping, and blade excitation can be exactly predicted.

The study of the structural response of the bladed-disk assembly includes the free and the forced vibration analysis of the structure. The free vibration analysis aims to determine structural dynamic characteristics of the bladed-disk assembly like the natural frequencies and the mode shapes. A review article by Leissa [LEIS 81] discusses the progress in modelling blades for vibration analysis. Various commercially available finite element codes have been employed for free vibration analysis. Substructuring techniques have also been used in the same problem ([SRIN 78], [EWIN 76]). Experimental research has also been performed, and the results have been found in good agreement with analytical ones [LEIS 84].

The forced vibration response problem has been considered much less. Rao [RAO 80], and Ewins [EWIN 80] gave detailed surveys on this subject. All studies treating the forced vibration problem assume that the blade forces are deterministic. The blade excitation is modeled as a periodic function in time with fundamental frequency equal to the rotation of the shaft or an integer multiple of this frequency. The forced vibration response is evaluated in the resonant cases, i.e., when one of the harmonics of the excitation is in resonance with one of the natural frequencies. The effect of the nonresonant harmonics is neglected. Recent work using the deterministic modelling of the forces was done by Jay et al. in [JAY 84]. Most of the forced vibration studies start from rather simple models for the blades. Griffin and Hoosac [GRIF 84] used a three-degree-of-freedom system for each blade. The mass and stiffness in this model are equal to the modal mass and stiffness of the blade in

the mode of interest. However, some work has been done recently using more refined blade models [RAO 80], [IRRE 84].

As mentioned earlier, the blade forces are assumed to be deterministic in current vibration studies. This is equivalent to the assumption that the characteristics of the flow around the blades are deterministic. However this is not true. The characteristics of the flow field are changing in a probabilistic fashion due to the turbulent nature of the flow. Some measurements of the flow fluctuations for an air-driven turbine have been performed and reported by Hodsan [HODS 85], [HODS 72].

From the data presented in these papers, it is shown that the randomly varying part of the velocity is of the same order of magnitude as the deterministic time-varying part. Furthermore, the statistical properties of the velocity, like for example its mean square, are periodic in time. Another source of randomness of the forces is the different degree of roughness of each blade surface, resulting from nonuniform deterioration of the blades. From the above, we conclude that the blade forces cannot be exactly predicted and therefore they should be modeled in a random fashion.

The blade force will be a randomly fluctuating function of time. A unique feature of the problem is the fact that the statistical properties of the force are varying periodically in time. Therefore, the excitation is a nonstationary process. The force is modeled as a nonstationary process with statistical properties varying periodically in time. The fundamental frequency of these periodic functions is equal to the frequency of rotation of the shaft or an integer multiple

of it. The random process representing the blade forces belongs to a class of stochastic processes that are called cyclostationary or periodically stationary. Furthermore the assembly can be considered as a multi-input, multi-output linear system. Inputs are the blade forces, and output is the blade response. The statistical properties and the response of linear systems driven by cyclostationary excitation have been studied quite extensively in statistical communication theory [GARD 75]. Nikolaidis studied the vibration of Marine Diesel engine propulsion shafting system under the random excitation of the cylinders and the propeller [NIKO 85A]. The problem studied there and the research have many common characteristics like the statistical nature of the excitation [NIKO 85B], [NIKO 87].

In this study we need to quantify the blade excitation in terms of its power spectral density function. Furthermore finding the correlation of the forces applied to each blade requires information on the spatial distribution of the velocity and pressure. A statistical description of turbulent flows in terms of the power spectral density of the pressure is given by Townsend in [TOWNS 76], Schlichting in [SCHL 79] and Schetz in [SCHETZ 84].

Measurements of spectra in turbulent boundary layers have been conducted by McGrath and Simpson [MCGR 87] and Blake [BLAKE 70]. Panton and Linebarger [PANT 74] did calculations on wall pressure spectra. Figure 5 depicts a smooth-wall pressure spectrum extracted from [BLAKE 70]. We see that the spectral density is given in terms of some dimensionless variables so it is fairly easy to get an

estimate of a spectrum for a specific case where the values of the parameters are specified.

Chapter 2. Modelling the Structure

2.1 Introduction

In this chapter we develop a simple dynamic model of a bladed-disk assembly (turbine/compressor). A 3-DOF model was given in a paper by Griffin and Hoosac [GRIF 84]. A simpler 2-DOF model is developed here using the data from the aformentioned paper. Though simple, this model approximates the response of a large mass of blades like for example 10 to 100 blades on one disk.

When the model for bladed-disk assembly was developed the sensitivity of the response to changes in the magnitudes of the forces applied from one blade to the other was investigated. This is analogous to the bladed-disk assembly which encounters almost equal forces, sinusoidal in time that differ only in phase from blade to blade. The forces are not equal because of imperfections in the geometry of the blades and variations of the flow field due to its turbulent nature.

The results of the sensitivity studies were encouraging, i.e., the structure was found to be sensitive to variations in applied forces. This is presented in the last segment of this chapter.

2.2 Dynamic Model for the Blade-Disk Assembly

This section deals with the problem of modelling a bladed-disk like a turbine or a compressor. A typical turbine or blade-disk assembly is shown in Fig. 6. We see that a large number of blades are fitted onto, or better into, a disk. At first glance we might think that a very complex model (high number of DOF's) would be needed to

represent the structure with reasonable accuracy. But because we are not so much interested in the response of one blade, but rather in the response of the whole system a relatively simple model with a small number of degrees of freedom (DOF) can serve that purpose.

If the stiffness or the flexibility of the structure were investigated we would see that the rotor disk itself is very stiff compared to the blades attached to it. Therefore one can justify the simplification that since it is not worth the effort to have any DOF's assigned to the rotor disk, the stiffness of the rotor disk is considered infinite.

This is exactly what is done in a paper by Griffin and Hoosac [GRIF 84]. The system is described by a model consisting of 3-DOF subsystem representing each blade. The lumped system of masses, springs, and dashpots depicted in Figure 7 is used to simulate one segment of the bladed disk. The parallel lines in Figure 6 indicate beam-like elements which have zero extensional flexibility and transverse flexibility.

The spring between the masses is used to represent coupling between blades. The information given for the values of the masses, springs and dashpots was used to derive a simpler 2-DOF model as shown in Figure 8. It is the same type of model with the one previously described and shown in Figure 7, except that the model for the blade has 2-DOF instead of 3. Also there are now two dashpots, connected with the two masses, instead of one. The dynamic properties of the 2-DOF system are determined so that the first two natural frequencies of the actual blades are equal to that of the 2-DOF system.

The equations of motion for the n^{th} blade and disk segment of the structure (Figure 8) are:

$$\begin{aligned} &m_1\ddot{X}_{1_i} + K_1(X_{1_i} - X_{2_i}) + C\dot{X}_{1_i} = F_i \\ &m_2\ddot{X}_{2_i} + K_1(X_{2_i} - X_{1_i}) + K_2X_{2_i} \\ &+ K_6(2X_{2_i} - X_{2_{(i+1)}} - X_{2_{(i-1)}}) + C\dot{X}_{2_i} = 0 \end{aligned} \qquad (2.1)$$

We have two masses, m_1 and m_2, three stiffnesses K_1, K_2 and the coupling K_6. To each of the masses a dashpot is connected. The displacement is denoted X_{1_i}, for the upper mass, and X_{2_i} for the lower mass. The coordinate system rotates with the blade. Centripotal and Coriolis effects are not considered in the model.

The external force is a combination of deterministic and random excitation. Chapter 3 is devoted to the modelling of the forces.

The model developed is relatively simple, only 2-DOF for each blade and therefore, it is feasible to simulate the free and forced dynamic response of the structure even for large number of blades without running into numerical difficulties.

The next section is a sensitivity analysis of the forced response of the above model when the forces are slightly varying.

2.3 Sensitivity of the Model

In this section we shall consider the question: "How is the response of the blades affected by the fact that the forces applied to each blade are not equal?" In other words, is the model sensitive to small variation in the forces from one blade to the other. Does a small variation in the input (forces) induce a higher or a lower

variation in the output (response)? If the variation is considerably magnified from the input to the output, this is an indication that the effect of randomness in the forces deserves further investigation. If not, either the dynamic model is not suitable to demonstrate the effect of randomness in the input, or this randomness is not important. A set of external forces with magnitudes and phases changing from blade to blade was assumed to be applied to the system. The amplitude of each force was assumed to be constant in time. The external force to each blade represents a particular engine order excitation. This excitation is caused by circumferential variations in the flow field around the blades which is a source of periodic excitation applied to the blades. The resulting forces can be represented by their Fourier series whose fundamental frequency equals to the angular frequency of rotation of the engine multiplied by the number of stators. In case that one of the harmonics of the excitation coincides with one of the natural frequencies of the bladed-disk assembly and the system is highly resonant we can ignore the nonresonant harmonics. The case studied had 20 blades (40 DOF) and the first natural frequency was found to be 448.9 rad/sec. Table 1 gives the values of the model parameters. The number of stators was set to be half the number of blades that is 10. The force acting on blade number n is:

$$F_n(t) = f_n e^{i(\omega_o t - 2\pi(n-1)S/N)} \qquad n = 1,2,\ldots,N \qquad (2.2)$$

The response of the system under this kind of excitation can be written as

$$\{X\} = [D(\omega_o)]^{-1} \{F\} \qquad (2.3)$$

where $\{F\}$ is the force vector, $[D(\omega_o)]^{-1}$ the inverse dynamic matrix and $\{X\}$ the displacement vector.

For the n^{th} blade, the response in a more compact form is:

$$X_n(t) = \sum_{k=1}^{N} d_{nk} f_k e^{i(\omega_o t - 2\pi(k-1)S/N)} \qquad (2.4)$$

The procedure of evaluating the response of the blades was repeated, each time for different levels of variability in the external forces. The results are presented in Table 2, where the coefficient of variation (ratio standard deviation over the mean) for the forces and the response is given. It is observed that the system is very sensitive to even small variations in the forces applied. A low coefficient of variation (C.O.V.) for the forces results in a much higher C.O.V. for the response. Even more important is the ratio of the maximum displacement to the displacement corresponding to the case that the excitation forces have equal amplitudes. As it can be observed from the same table the displacement increases dramatically even for small variations in the magnitudes of the applied forces.

In conclusion a more detailed analysis of the response of the system that accounts for the variability in the exciting forces is a task that is worth undertaking.

In the next chapters the problem of modelling the excitation and estimating the resulting displacements of the blades will be studied.

Chapter 3. Modelling the Blade Forces

3.1 Introduction

In this chapter, a statistical model of the forces acting on the blades is developed. The model is one dimensional and it describes the force applied at a fixed point on the blade as a function of time.

The airfoil of the blade is modelled as a flat-plate airfoil, [KARA 66], and the coefficient of lift is considered to be a linear function of the angle of attack, as shown in Figure 9. The blade force is linearized with respect to velocity toward its mean value in order to further simplify the approach. Thereafter the cross-correlation for the forces is evaluated. To do that some information is needed about the cross-correlation of the velocity encountered by each individual blade. In this study, a correlation function of exponential type is assumed for both the temporal and spatial variations of the inflow velocity when it is measured with respect to a fixed coordinate system.

Having developed a simple model for the blade forces and their correlation the next step is to solve the input-output problem and evaluate the response. A unique feature of this model is the statistical periodicity of the blade forces called cyclostationary. The statistics of the velocity are periodic and that explains why the statistics of the forces have the same property. The cyclostationary property is preserved from the input to the output. Chapter 4 deals with solving the input-output problem.

3.2 Blade Forces

3.2.1 Forces

First how we can evaluate a lift on an airfoil? By applying the Kutta condition for an airfoil, it can be shown that the lift is:

$$F_L = 4\pi\rho V_\infty^2 a \sin(\alpha + \beta) \tag{3.1}$$

where a is the radius of the circle that the Kutta condition was applied on. The lift on the airfoil is zero when the angle of attack (AOA) is equal to $-\beta$. This is called the zero-lift angle. Consequently the lift coefficient is:

$$C_L = \frac{F_L}{\frac{1}{2}\rho V_\infty^2 \ell} = 8\pi\left(\frac{a}{\ell}\right) \sin(\alpha + \beta) \tag{3.2}$$

For the limiting case of a flat plate airfoil the chord, ℓ, is about $4a$. Furthermore if we assume small angles of attack the lift coefficient can be expressed as:

$$C_L = 2\pi(\alpha + \beta) \tag{3.3}$$

Figure 9 shows that this linear approximation is acceptable within a reasonable range of values of the AOA.

As seen in Figure 10, V_∞ can be decomposed into two orthogonal components, V_X and V_Y, of which V_X is parallel to the airfoil. The figure also shows that α is a function of V_X and V_Y i.e.

$$\alpha = \tan^{-1}\left(\frac{V_Y}{V_X}\right) \tag{3.4}$$

Again if we assume small AOA the lift coefficient can be expressed as

$$C_L = 2\pi\left[\frac{V_Y}{V_X} + \beta\right] \tag{3.5}$$

Finally the lift force is given by

$$F_L = \rho\pi\ell(V_X^2 + V_Y^2)\left[\frac{V_Y}{V_X} + \beta\right] \tag{3.6}$$

Because we are always assuming a small AOA, the free stream velocity is close to the velocity parallel to the airfoil, and therefore we write:

$$F_L = \rho\pi\ell\left[\beta V_X^2 + V_X V_Y\right] \tag{3.7}$$

We have expressed the lift on an airfoil or a blade in terms of the components of the velocity of the flow encountered by the blade, V_X and V_Y.

In a turbomachinery layup things get more involved. The following applies for a turbine. The axial flow has to pass through a stator stage that will change slightly the direction of the flow in a way that it hits the turbine blades at a prescribed AOA. The velocity triangles for a turbine stage are depicted in Figure 11. Due to the turbulent nature of the axial flow an additional component, V_i^*, is needed to be added to the free stream velocity V_i to account for the effect of turbulence.

In order to evaluate the force of each blade we consider eq. (3.7) in which the force is expressed as a function of V_X and V_Y. These last two components can be expressed in terms of the velocities V_i and V_i^* as follows:

$$V_X = V_X(V_i, V_i^*) \text{ and}$$
$$V_Y = V_Y(V_i, V_i^*) \tag{3.8}$$

Therefore the lift force can also be expressed as a function of V_i and V_i^*:

$$F_L = F_L(V_i, V_i^*) \tag{3.9}$$

The next step is to find V_X and V_Y:

$$V_X = V_{rel_1}\cos(\alpha + \alpha_1) ,$$

$$V_Y = V_{rel_1} \sin(\alpha + \alpha_1) \tag{3.10}$$

where V_{rel_1} is the instantaneous relative velocity as seen by the rotor blade. With the aid of Figure 11 it can be shown that:

$$V_{rel_1}^2 = V_i^2 + V_i^{*2} + (\omega r)^2 + 2\omega r(V_i^* \cos\theta_1 - V_i \sin\theta_1) \tag{3.11}$$

where θ_1 is the angle of the blades of the stator. We also need the instantaneous angle of attack. From Figure 12 it can be shown that:

$$(\alpha + \alpha_1) = \tan^{-1}\left[\frac{(\omega r) - \bar{V}_i \sin\theta_1}{\bar{V}_i \cos\theta_1}\right] + \alpha_1 - \tan^{-1}\left[\frac{(\omega r) - V_i \sin\theta_1 + V_i^* \cos\theta_1}{V_i \cos\theta_1 + V_i^* \sin\theta_1}\right] \tag{3.12}$$

Everything is now known to evaluate the lift force on each blade. Unfortunately the expressions derived here are nonlinear. In order to simplify the expression for the lift force is linearized with respect to the velocities V_i and V_i^*.

3.2.2 Linearization

Expanding the expression for the blade force around the point $(\bar{V}_i, 0)$ and neglecting higher than second order terms we obtain the following expression for the force applied to the k^{th} blade:

$$\begin{aligned} F_k(t) &= F(V_{i_k}(t), V_{i_k}^*(t)) \\ &\approx F(\bar{V}_i, 0) + \left.\frac{\partial F}{\partial V_{i_k}}\right|^{\circ} (V_{i_k}(t) - \bar{V}_i) \\ &\quad + \left.\frac{\partial F}{\partial V_{i_k}^*}\right|^{\circ} V_{i_k}^*(t) \end{aligned} \tag{3.13}$$

Figure 12 shows how the inflow velocity V_i and the perpendicular inflow velocity V_i^* behave with time.

V_i is fluctuating periodically around $\bar{V}_i$. On top of that we have a random fluctuation ($\alpha_k(t)P_{2_k}(t)$) around the periodic part ($P_{1_k}(t)$). V_i^* is fluctuating randomly around the mean value zero. The random fluctuation can be written, as a product of a random function $\gamma_k(t)$, and a periodic function $P_{2_k}(t)$ that expands or constrains the fluctuation depending on whether the velocity is measured behind a stator blade (wake) or in between blades.

The velocities encountered by the k^{th} blade are then:

$$V_{i_k}(t) = P_{1_k}(t) + \alpha_k(t)P_{2_k}(t)$$
$$v^*_{i_k}(t) = \gamma_k(t)P_{2_k}(t) \qquad (3.14)$$

Getting back to the linearization it simplifies things to write:

$$F_{1_k} = F(\bar{V}_i, 0)$$
$$\Delta F_{i_k} = \frac{\partial F}{\partial V_{i_k}}\Big|^{\circ}$$
$$\Delta F^*_{i_k} = \frac{\partial F}{\partial V^*_{i_k}}\Big|^{\circ} \qquad (3.15)$$

When we subtract $\bar{V}_i$ from $V_{i_k}(t)$ in (3.14) we get

$$\tilde{P}_{1_k}(t) = P_{1_k}(t) - \bar{V}_i \qquad (3.15)$$

$\tilde{P}_{1_k}(t)$ has the mean value zero. Finally, the linearized lift force to the k^{th} blade can be written as:

$$F_k(t) = F_{1_k} + \Delta F_{i_k}(\tilde{P}_{1_k}(t) + \alpha_k(t)P_{2_k}(t)) + \Delta F^*_{i_k}(\gamma_k(t)P_{2_k}(t)) \qquad (3.16)$$

3.3 Statistical model of the blade forces

3.3.1 Velocities

In a turbulent flow the velocity measured with respect to a fixed coordinate system, is changing randomly in both time and space. Therefore in this particular problem the inflow velocity V_i is a four dimensional random field, the first three dimensions corresponding to the three spatial coordinates and the fourth to the time. Consider a cylindrical coordinate system, that is fixed in space with its origin located at the center of the disk as that in Figure 13. The following assumptions are made regarding the velocity field $V_i(r,\theta,Z,t)$:

a) The velocity does not change significantly in the radial direction.

b) Considering the velocity on a plane just in front of the disk the Z coordinate becomes unimportant.

According to the above assumptions the velocity can be considered as a function of the space coordinate θ and the time. In the following the two dimensional velocity field will be defined in terms of its correlation function. The next step will be to derive the statistics of the relative velocity field viewed from a relative coordinate system attached to a blade. Finally the attention will focus to the forces applied to the blades. Each of these forces is a random function of time. The statistics of these random processes will be derived from the statistics of the velocity field and the linearized relations between forces and velocities of the previous sections.

The inflow velocity can be written as a function of t and θ, $V_{i_k}(t,\theta)$ in stator K and for the velocity perpendicular to this inflow velocity. The following equations are suggested:

$$V_{i_k}(t,\theta) = P_{1_k}(\theta) + \alpha_k'(t,\theta)P_{2_k}(\theta)$$
$$V^*_{i_k}(t,\theta) = \gamma_k'(t,\theta) + P_{2_k}(\theta) \qquad (3.17)$$

where $P_{1_k}(\theta)$ and $P_{2_k}(\theta)$ are periodic in θ, $\alpha_k(t,\theta)$ and $\gamma_k(t,\theta)$ are random fluctuations with the mean zero. Many forms of correlation functions do exist, but they nearly always have one thing in common, an exponential decay. Therefore in this study a correlation function for both time and space of exponential form is suggested:

$$R_{\alpha'}(\tau,\Delta\theta) = \sigma_\alpha^2 e^{-C_1|\tau|}\, e^{-C_2|\Delta\theta|}$$
$$R_{\gamma'}(\tau,\Delta\theta) = \sigma_\gamma^2 e^{-C_3|\tau|}\, e^{-C_4|\Delta\theta|} \qquad (3.18)$$

where σ_α and σ_γ are the standard derivations of the velocities. The constants C_1 and C_2 have to do with the scale of turbulence in the time and space. If C_1 is measured in seconds it tells us what the correlation is for a time difference of one second. Similarly if C_2 is measured in millimeters it gives the correlation for a distance of one millimeter. Therefore it is related to the scale of turbulence, bigger scale means a higher correlation than else. C_3 and C_4 are defined in the same way.

Next consider the k^{th} blade, the spatial coordinate θ for that blade is:

$$\theta = \omega_o rt - \frac{2\pi r}{N}(k-1)\ ,\ N \text{ number of blades}$$

or

$$\theta = \omega_o rt - \theta_k \qquad (3.19)$$

Substitute (3.19) into equation (3.17) so the velocities are now functions of time only:

$$V_{i_k}(t) = P_{1_k}(t) + \alpha_k'(t,\omega_o rt-\theta_k)P_{2_k}(t)$$

$$V^*_{i_k}(t) = \gamma_k'(t,\omega_o rt-\theta_k)P_{2_k}(t)$$

Simplify

$$\alpha_k'(t,\omega_o rt-\theta_k) = \alpha_k(t) \qquad \bar{\alpha}_k(t) = 0$$

$$\gamma_k'(t,\omega_o rt-\theta_k) = \gamma_k(t) \qquad \bar{\gamma}_k(t) = 0$$

This result gives correlation functions only in time.

$$R_{\alpha_k}(\tau) = \sigma_\alpha^2 e^{-C_1|\tau|} e^{-C_2\omega_o r|\tau|}$$

$$R_{\gamma_k}(\tau) = \sigma_\gamma^2 e^{-C_3|\tau|} e^{-C_4\omega_o r|\tau|} \qquad (3.20)$$

What about cross-correlation? We can write the cross-correlation between blades k and ℓ, see Figure 13, as

$$R_{\alpha_k\alpha_\ell}(\tau) = E[\alpha_k(t_1)\alpha_\ell(t_2)]$$

where

$$\alpha_k(t_1) = \alpha'(t_1,\omega_o rt_1-2\pi rS(k-1)/N)$$

$$\alpha_\ell(t_2) = \alpha'(t_2,\omega_o rt_2-2\pi rS(\ell-1)/N)$$

Therefore the cross-correlation between blades k and ℓ turns out to be:

$$R_{\alpha_k\alpha_\ell}(\tau) = \sigma_\alpha^2 e^{-(C_1 + C_2\omega_o r)|\tau|} e^{-(2\pi rS|k-\ell|/N)} \qquad (3.21)$$

The form is the same for the perpendicular velocity cross-correlation:

$$R_{\gamma_k\gamma_\ell}(\tau) = \sigma_\gamma^2 e^{-(C_3+C_4\omega_o r)|\tau|} e^{-(2\pi rS|k-\ell|/N)} \qquad (3.22)$$

It is assumed that no correlation exists between the parallel and the perpendicular velocity components:

$$R_{\alpha_k \gamma_\ell}(\tau) = 0$$

This is only a good assumption if $-\overline{V_\alpha V_\gamma} \approx 0$.

3.3.2 Forces

In Eq. (3.16) we have the linearized blade force on blade number k. The cross-correlation between blade force p and blade force q is then:

$$\begin{aligned} &E[F_p(t_1)F_q(t_2)] \\ &= E\Big[\Big(F_{1_p} + \Delta F_{i_p}\big(\tilde{P}_{1_p}(t_1) + \alpha_p(t_1)P_{2_p}(t_1)\big) + \Delta F^*_{i_p}\big(\gamma_p(t_1)P_{2_p}(t_1)\big)\Big) \\ &\times \Big(F_{1_q} + \Delta F_{i_q}\big(\tilde{P}_{1_q}(t_2) + \alpha_q(t_2)P_{2_q}(t_2)\big) + \Delta F^*_{i_q}\big(\gamma_q(t_2)P_{2_q}(t_2)\big)\Big)\Big] \end{aligned} \tag{3.23}$$

The next step is to do the algebra and cancel out terms that have the expected value zero. After doing this we end with:

$$\begin{aligned} R_{F_p F_q}(t_1,t_2) &= F_{1_p} F_{1_q} \\ &+ \Delta F_{i_p} \Delta F_{i_q} \tilde{P}_{1_p}(t_1)\tilde{P}_{1_q}(t_2) + \Delta F_{i_p} \Delta F_{i_q} P_{2_p}(t_1)P_{2_q}(t_2)E[\alpha_p(t_1)\alpha_q(t_2)] \\ &+ \Delta F^*_{i_p} \Delta F^*_{i_q} P_{2_p}(t_1)P_{2_q}(t_2)E[\gamma_p(t_1)\gamma_q(t_2)] \end{aligned} \tag{3.24}$$

When the cross-correlation between the blade forces has been solved, Eq. (3.24), the response for the bladed-disk assembly can be evaluated. That is what chapter 4 concentrates on.

Chapter 4 Evaluation of the Statistics of the Response: The Input-Output Problem

4.1 Introduction

In this chapter the response of the blades is evaluated. According to the assumptions of the previous chapter the problem consists of determining the statistical properties of the output of a linear system driven by multiple, random inputs. The linear system is the blade-disk assembly, the inputs are the forces, and the outputs are the displacements of the blades. The solution of the problem is based on the following assumptions:

(i) For the nonresonant case, the displacement of the blades is negligible compared with the displacement under resonant conditions.

(ii) In case of resonance, the nonresonant harmonics of the excitation can be neglected in the evaluation of the displacement.

These assumptions are based on the following, quoted from Griffins paper [GRIF 84].

> "The external force represents a particular engine order excitation and, as a result, is sinusoidal in time and differs only in phase from blade to blade. This type of variation is caused by circumferential variations in the flow field which translate into a source of periodic excitation in the reference frame of the rotating blades. The resulting forcing function is equivalent to a Fourier series which has frequencies proportional to integer multiples of the engine rpm. As the engine changes speed, one of these frequencies may coincide with a natural frequency of the bladed disk at which time the other terms in the Fourier series have little effect and are negligible. Under these circumstances each blade is exposed to the same excitation except for differences in phase which are proportional to the blade's circumferential position on the disk."

Under these assumptions, the excitation on the blade forces can be considered Gaussian, amplitude modulated (AM) processes with a fixed phase relationship between the carriers. The carrier frequency equals the system natural frequency in resonance and the modulated amplitudes are Gaussian processes with known autocorrelation and cross-correlation functions. These have been established in the previous chapter.

The approach used here to determine the output statistics utilizes the fact that the input processes are wide since cyclostationary [PAPO 83], [NIKO 85A], [NIKO 87]. A random process is called wide sense cyclostationary if its mean and its autocorrelation function, $R(t+\tau,t)$ are periodic in t [PAPO 83]. This class of processes have been studied, see [HURD 69], [OGUR 71], [GUDZ 59], [GLAD 63].

The problem is solved in its general form by deriving an expression relating the double Fourier transform at the output autocorrelation function with the double Fourier transform of the input autocorrelation and cross-correlation functions.

It is shown that the response is a cyclostationary process. Therefore the cyclostationary property is preserved from the input to the output. Futhermore, the frequency of the second moment of the response is equal to two times the frequency of the excitation. The results are then used to evaluate the displacements due to deterministic and random excitation. By comparing the mean squares of the response due to the random part of the exciting force and that due to the deterministic part, we can assess the importance of accounting

for the random nature of the flow field around the blades. The results from such a comparison are discussed in chapter 5.

4.2 Analysis of the General Input-Output Problem

Consider a multi-input, time-invariant linear system whose inputs are the amplitude-modulated processes $S_i(t)$, i=1,...,N, which have the same carrier frequency ω_o and whose output is the random process r(t). The transfer matrix is an Nx1 row vector (see Figure 14) with elements $H_i(\omega)$, i=1,...,N. The inputs can be written as

$$S_i(t) = a_i(t) \cos(\omega_o t - \phi_i), \quad i=1,\ldots,N \tag{4.1}$$

where $a_i(t)$ is the modulated amplitude of the i^{th} input or

$$S_i(t) = a_i(t)(C_i e^{j\omega_o t} + C_i^* e^{-j\omega_o t}), \quad i=1,\ldots,N \tag{4.2}$$

where

$$C_i = \frac{\cos\phi_i - j \sin\phi_i}{2} \tag{4.3}$$

Assume that the modulated amplitudes are jointly stationary Gaussian processes. The input-output problem will be solved first for the case where the means of the modulated amplitudes are zero. The results can then be easily extended for the case where the means are nonzero. The cross-correlation function of $S_i(t)$ and $S_k(t)$ is

$$\begin{aligned} R_{S_i S_k}(t+\tau,t) = {} & C_{a_i a_k}(\tau)(C_i C_k^* e^{j\omega_o\tau} + C_i^* C_k e^{-j\omega_o\tau}) \\ & + C_{a_i a_k}(\tau) C_i C_k e^{j\omega_o\tau} e^{2j\omega_o t} \\ & + C_{a_i a_k}(\tau) C_i^* C_k^* e^{-j\omega_o\tau} e^{-2j\omega_o t} \end{aligned}$$

$$\text{for } i,k=1,\ldots,N \text{ and } i \neq k \tag{4.4}$$

Where $C_{a_i a_k}(\tau)$ is the cross-covariance of $a_i(t)$ and $a_k(t)$. The autocorrelation function of $S_i(t)$, i=1,...,N can be obtained form equation (4.4) if we put i=k. The autocorrelations and the cross-correlations are periodic in t with period π/ω_o; that is, half of the carrier period. Since the mean of $S_i(t)$ is zero, the random processes $S_i(t)$, i=1,...,N are cyclostationary, [PAPO 83], [FRANK 69].

The double Fourier transform of $R_{S_i S_k}(t+\tau,t)$ with respect to t and τ is defined as follows:

$$\Delta_{S_i S_k}(\omega_1,\omega_2) = \int_{-\infty}^{+\infty}\int_{-\infty}^{+\infty} R_{S_i S_k}(t+\tau,t)e^{-j(\omega_1\tau-\omega_2 t)}\,d\tau dt \qquad (4.5)$$

hence

$$R_{S_i S_k}(t+\tau,t) = \frac{1}{(2\pi)^2}\int_{-\infty}^{+\infty}\int_{-\infty}^{+\infty} \Delta_{S_i S_k}(\omega_1,\omega_2)e^{j(\omega_1\tau-\omega_2 t)}\,d\omega_1 d\omega_2 \qquad (4.6)$$

If the function $R_{S_i S_k}(t+\tau,t)$ is absolutely integrable in the t,τ - plane, then its double transform $\Delta_{S_i S_k}(\omega_1,\omega_2)$ exists for all ω_1 and ω_2 and is bounded. The double transform can still be defined if $R_{S_i S_k}(t+\tau,t)$ is not absolutely integrable. However, this function will contain singularities in the form of delta functions.

The statistics of the output can be found by using the following result (Appendix) for the double Fourier transform of the autocorrelation of the response r(t) of an N-input time-invariant linear system with respect to t and τ:

$$\Delta_r(\omega_1,\omega_2) = \sum_{i=1}^{N}\sum_{k=1}^{N} \Delta_{S_i S_k}(\omega_1,\omega_2)H_i(\omega_1)H_k^*(\omega_1+\omega_2) \qquad (4.7)$$

where $\Delta_{S_i S_k}(\omega_1,\omega_2)$ is generalized spectral density or the double Fourier transform of $R_{S_i S_k}(t+\tau,t)$. Using equations (4.4) and (4.5) we obtain

$$\begin{aligned}\Delta_{S_i S_k}(\omega_1,\omega_2) = 2\pi\delta(\omega_2)\{&C_i C_k^* S_{a_i a_k}(\omega_1-\omega_o) \\ &+ C_i^* C_k S_{a_i a_k}(\omega_1+\omega_o) \\ &+ 2\pi C_i C_k S_{\alpha_i \alpha_k}(\omega_1-\omega_o)\delta(\omega_2+2\omega_o) \\ &+ 2\pi C_i^* C_k^* S_{a_i a_k}(\omega_1+\omega_o)\delta(\omega_2-2\omega_o)\} \text{ for } i,k=1,\ldots,N\end{aligned} \tag{4.8}$$

where $S_{a_i a_k}(\omega)$ denotes the cross-spectral density of $a_i(t)$ and $a_k(t)$ if $i\neq k$ and the auto-spectral density of $a_i(t)$ if $i=k$.

The double Fourier transform of the autocorrelation of r(t) can be obtained by using equations (4.7) and (4.8):

$$\begin{aligned}\Delta_r(\omega_1,\omega_2) = {} & 2\pi\delta(\omega_2)\sum_{i=1}^{N}\sum_{k=1}^{N} C_i C_k^* S_{a_i} S_{a_k}(\omega_1-\omega_o) \\ & \times H_i(\omega_1)\, H_k^*(\omega_1+\omega_2) + 2\pi\delta(\omega_2)\sum_{i=1}^{N}\sum_{k=1}^{N} C_i^* C_k S_{a_i a_k}(\omega_1+\omega_o) \\ & H_i(\omega_1)H_k^*(\omega_1+\omega_2) + 2\pi\delta(\omega_2+2\omega_o) \\ & \times \sum_{i=1}^{N}\sum_{k=1}^{N} C_i C_k S_{a_i a_k}(\omega_1-\omega_o)H_i(\omega_1)H_k^*(\omega_1+\omega_2) \\ & + 2\pi\delta(\omega_2-2\omega_o)\sum_{i=1}^{N}\sum_{k=1}^{N} C_i^* C_k^* S_{a_i a_k}(\omega_1+\omega_o) \\ & \times H_i(\omega_1)H_k^*(\omega_1+\omega_2)\end{aligned} \tag{4.9}$$

The autocorrelation function of r(t) is now obtained by taking the inverse Fourier transform of $\Delta r(\omega_1,\omega_2)$ as given by equation (4.9):

$$R_r(t+\tau,t) = \frac{1}{2\pi}\sum_{i=1}^{N}\sum_{k=1}^{N}\int_{-\infty}^{+\infty} C_i C_k^* S_{a_i a_k}(\omega_1-\omega_o)H_i(\omega_1)$$

$$x\ H_k^*(\omega_1)\cdot e^{j\omega_1\tau}\,d\omega_1 + \frac{1}{2\pi}\sum_{i=1}^{N}\sum_{k=1}^{N}\int_{-\infty}^{+\infty} C_i^* C_k$$

$$x\ S_{a_i a_k}(\omega_1+\omega_o)H_i(\omega_1)H_k^*(\omega_1)\cdot e^{j\omega_1\tau}\,d\omega_1$$

$$+ \frac{1}{2\pi}\sum_{i=1}^{N}\sum_{k=1}^{N}\int_{-\infty}^{+\infty} C_i C_k S_{a_i a_k}(\omega_1-\omega_o)H_i(\omega_1)$$

$$x\ H_k^*(\omega_1-2\omega_o)\cdot e^{j\omega_1\tau}\, e^{2j\omega_o t}\,d\omega_1$$

$$+ \frac{1}{2\pi}\sum_{i=1}^{N}\sum_{k=1}^{N}\int_{-\infty}^{+\infty} C_i^* C_k^* S_{a_i a_k}(\omega_o+\omega_1)H_i(\omega_1)$$

$$x\ H_k^*(\omega_1+2\omega_o)\cdot e^{j\omega_1\tau}\, e^{-2j\omega_o t}\,d\omega_1 \qquad (4.10)$$

After some algebraic manipulations we obtain:

$$R_r(t+\tau,t) = e^{j\omega_o t}A(\tau) + e^{-j\omega_o\tau}A^*(\tau)$$

$$+ e^{j\omega_o\tau}e^{2j\omega_o t}B(\tau) + e^{-j\omega_o\tau}e^{-2j\omega_o t}B^*(\tau)$$

where

$$A(\tau) = \frac{1}{2\pi}\sum_{i=1}^{N}\sum_{k=1}^{N}\int_{-\infty}^{+\infty} C_i C_k^* S_{a_i a_k}(\omega_3)H_i(\omega_3+\omega_o)$$

$$x\ H_k^*(\omega_3+\omega_o)\cdot e^{j\omega_3\tau}\,d\omega_3$$

and

$$B(\tau) = \frac{1}{2\pi}\sum_{i=1}^{N}\sum_{k=1}^{N}\int_{-\infty}^{+\infty} C_i C_k S_{a_i a_k}(\omega_3)H_i(\omega_3+\omega_o)$$

$$x\ H_k^*(\omega_3-\omega_o)\cdot e^{j\omega_3\tau}\,d\omega_3 \qquad (4.11)$$

4.3 Solution for the Deterministic Excitation

Equation (3.24), developed in chapter 3, yields the autocorrelation and cross-correlation of the exciting forces, for both the deterministic and random part.

The deterministic part is:

$$R^{D}_{F_pF_q}(t_1,t_2) = F_{1_p} F_{1_q} + \Delta F_{i_p} \Delta F_{i_q} \tilde{P}_{1_p}(t_1)\tilde{P}_{1_q}(t_2).$$

Another way to write this expression is:

$$\begin{aligned} R^{D}_{F_pF_q}(t+\tau,t) &= F_{1_p} F_{1_q} \\ &+ \Delta F_{i_p} \Delta F_{i_q} a^2\{\tilde{C}_{1_p} \tilde{C}_{1_q} e^{j\omega_o\tau} e^{j2\omega_o t} + \tilde{C}_{1_p} \tilde{C}_{1_q}^{*} e^{j\omega_o\tau} \\ &+ \tilde{C}_{1_p}^{*}\tilde{C}_{1_q} e^{-j\omega_o\tau} + \tilde{C}_{1_p}^{*}\tilde{C}_{1_q}^{*} e^{-j2\omega_o t} e^{-j\omega_o\tau}\} \end{aligned} \tag{4.12}$$

See equation (4.1) through (4.4).

The double Fourier transformations of $R^{D}_{F_pF_q}(t+\tau,t)$ is given in equation (4.5). The result is:

$$\begin{aligned} \Delta^{D}_{F_pF_q}(\omega_1,\omega_2) &= F_{1_p} F_{1_q} (2\pi)^2\delta(-\omega_1)\delta(\omega_2) \\ &+ \Delta F_{i_p} \Delta F_{i_q} a^2(2\pi)^2\{\tilde{C}_{1_p} \tilde{C}_{1_q} \delta(\omega_o-\omega_1)\delta(2\omega_o+\omega_2) \\ &+ \tilde{C}_{1_p} \tilde{C}_{1_q}^{*} \delta(\omega_o-\omega_1)\delta(\omega_2) \\ &+ \tilde{C}_{1_p}^{*}\tilde{C}_{1_q} \delta(-\omega_o-\omega_1)\delta(\omega_2) \\ &+ \tilde{C}_{1_p}^{*}\tilde{C}_{1_q}^{*} \delta(-\omega_o-\omega_1)\delta(-2\omega_o+\omega_2)\} \end{aligned} \tag{4.13}$$

The statistics of the output can be found by using equation (4.7):

$$\Delta^{D}_{r}(\omega_1,\omega_2) = \sum_{i=1}^{N}\sum_{k=1}^{N} \Delta^{D}_{F_iF_k}(\omega_1,\omega_2) H_i(\omega_1) H_k^{*}(\omega_1+\omega_2)$$

The autocorrelation function for the deterministic part of the response is now obtained by taking the inverse Fourier transform of $\Delta^{D}_{r}(\omega_1,\omega_2)$, see equation (4.6), and the following result is obtained:

$$R_r^D(t+\tau,t) = (F_1)^2 \sum_{i=1}^{N}\sum_{k=1}^{N} H_i(0)H_k^*(0)$$
$$+ (\Delta F_i)^2 a^2 \sum_{i=1}^{N}\sum_{k=1}^{N} \{\tilde{C}_{1_i}\tilde{C}_{1_k} H_i(\omega_o)H_k^*(-\omega_o)e^{j2\omega_o t}e^{j\omega_o\tau}$$
$$+ \tilde{C}_{1_i}\tilde{C}_{1_k}^* H_i(\omega_o)H_k^*(\omega_o)e^{j\omega_o\tau}$$
$$+ \tilde{C}_{1_i}^*\tilde{C}_{1_k} H_i(-\omega_o)H_k^*(-\omega_o)e^{-j\omega_o\tau}$$
$$+ \tilde{C}_{1_i}^*\tilde{C}_{1_k}^* H_i(-\omega_o)H_k^*(\omega_o)e^{-j2\omega_o t}e^{-j\omega_o\tau}\} \qquad (4.14)$$

4.4 Solution for the Random Excitation

As mentioned earlier, the auto- and cross-correlation for the input (forces) is given by (3.24):

$$R_{F_pF_q}^R(t_1,t_2) = \Delta F_{i_p}\Delta F_{i_q} P_{2_p}(t_1)P_{2_q}(t_2)E[\alpha_p(t_1)\alpha_q(t_2)]$$
$$+ \Delta F_{i_p}^*\Delta F_{i_q}^* P_{2_p}(t_1)P_{2_q}(t_2)E[\gamma_p(t_1)\gamma_q(t_2)]$$

Another way to write this expression is:

$$R_{F_pF_q}^R(t+\tau,t) = \Delta F_{i_p}\Delta F_{i_q} C_{\alpha_p\alpha_q}(\tau)$$
$$\times \{C_{2_p}C_{2_q}e^{j\omega_o\tau}e^{j2\omega_o t} + C_{2_p}C_{2_q}^* e^{j\omega_o\tau}$$
$$+ C_{2_p}^* C_{2_q} e^{-j\omega_o\tau} + C_{2_p}^* C_{2_q}^* e^{-j2\omega_o t}e^{-j\omega_o\tau}\}$$
$$+ \Delta F_{i_p}^*\Delta F_{i_q}^* C_{\gamma_p\gamma_q}(\tau)$$
$$\times \{C_{2_p}C_{2_q}e^{j\omega_o\tau}e^{j2\omega_o t} + C_{2_p}C_{2_q}^* e^{j\omega_o\tau}$$
$$+ C_{2_p}^* C_{2_q} e^{-j\omega_o\tau} + C_{2_p}^* C_{2_q}^* e^{-j2\omega_o t}e^{-j\omega_o\tau}\} \qquad (4.15)$$

where $C_{\alpha_p\alpha_q}(\tau)$ and $C_{\gamma_p\gamma_q}(\tau)$ are given by (3.21) and (3.22) respectively. In section 4.1 the general input-output problem was

solved. Equation (4.15) has the same form as equation (4.4). Therefore it is not necessary to go through the solution process again. Instead just apply the result as given in equation (4.11), where the auto-correlation function is:

$$R_r^R(t+\tau,t) = (\Delta F_i)^2\{A(\tau)e^{j\omega_o\tau} + A^*(\tau)e^{-j\omega_o\tau} + B(\tau)e^{j\omega_o\tau}e^{j2\omega_o t} + B^*(\tau)e^{-j\omega_o\tau}e^{-j2\omega_o t}\} + (\Delta F_i^*)^2\{X(\tau)e^{j\omega_o\tau} + X^*(\tau)e^{-j\omega_o\tau} + Y(\tau)e^{j\omega_o\tau}e^{2j\omega_o t} + Y^*(\tau)e^{-j\omega_o\tau}e^{-j2\omega_o t}\}$$

where

$$A(\tau) = \frac{1}{2\pi}\sum_{i=1}^{N}\sum_{k=1}^{N}\int_{-\infty}^{+\infty} C_2\, C_2^*\, S_{\alpha_i\alpha_k}(\omega_3) \cdot x\, H_i(\omega_3+\omega_o)H_k^*(\omega_3+\omega_o)e^{j\omega_3\tau}\, d\omega_3 .$$

and

$$B(\tau) = \frac{1}{2\pi}\sum_{i=1}^{N}\sum_{k=1}^{N}\int_{-\infty}^{+\infty} C_2\, C_2^*\, S_{\alpha_i\alpha_k}(\omega_3) \cdot x\, H_i(\omega_3+\omega_o)H_k^*(\omega_3-\omega_o)e^{j\omega_3\tau}\, d\omega_3 \qquad (4.17)$$

The same expression is used for $X(\tau)$ as for $A(\tau)$, but instead of α it is now γ. The same exchange is for $B(\tau)$ and $Y(\tau)$. The spectrum for the inflow parallel velocity $S_{\alpha_i\alpha_k}(\omega)$ is obtained from (3.21) by taking the Fourier transform of the autocorrelation function. The result is:

$$S_{\alpha_i\alpha_k}(\omega) = \frac{\sigma_\alpha^2}{\pi}\,\frac{(C_1 + C_2 r\omega_o)}{\omega^2 + (C_1 + C_2 r\omega_o)^2}\cdot e^{-C_2|i-k|\frac{2\pi rS}{N}} \qquad (4.18)$$

The same form is used for the γ-spectrum.

Chapter 5 Examples

5.1 Introduction

In Chapter 2, a simple dynamic model for the blade-disk assembly was developed. The sensitivity of the model was tested and the results are given in section 2.3. It was shown that the model is very sensitive to a small variability in the input (forces) and that the resulting variability in the output (response) is much higher. When the sensitivity was tested, we varied only the amplitude of the forces from blade to blade, but for each blade the amplitude was assumed to be constant with time.

In practice this is not true. Therefore a more refined approach was developed in Chapter 3 to take into account the change of amplitude with time. A one-dimensional model describing the force applied at a fixed point on the blade, as a function of time, was developed. The Input-Output problem was solved i.e. the response of the blades was evaluated in Chapter 4.

In this chapter some examples of evaluating the response of the blades due to random exciting forces are studied. The results obtained for an approach, based on the model developed, are presented and discussed. A comparison of the response due to the random and the deterministic part of the calculated response of the blades, reveals the significance of the variability in the blade forces. The second-order statistics have been evaluated and the results are given in Figures 15 through 20.

The root mean square value (RMS) of the response is changing with time, due to its nonstationary character. In the examples studied the results indicate that the standard deviation, due to the random part, may become as high as 35% of the maximum value of the deterministic part. This is a significant effect and must be considered when designing the system. This effect can be even stronger in other cases.

5.2 Results and Discussions

The model was tested using some values for the parameters involved in the model that are close to what we expect in a real situation. The Test Case Data can be seen in Table 3. The driving frequency was selected as the first normal frequency of the bladed-disk assembly. This corresponds to 429 rpm, which is not very high for a turbine. However this can be encountered during a transient operation of a turbine. There are also turbines that operate at a low rpm, Hodson [HODS 85] made measurements for a air-turbine rotating at 530 rpm. The rotational speed typically varies between 400 and 40,000 rpm. The selected values of the velocities and the blade angles are typical of real situation, see [OATES 84] and [KERR 77]. The mean inflow velocity $\overline{V_i}$ is set equal to 300 m/s and the mean for the perpendicular velocity $\overline{V_i^*}$ is 0 m/s. The mean angle of attack α, is 0° and the stator blade angle θ_1 is selected as 60. We set the zero lift angle β, equal to 5° and calculated that the mean relative flow

angle β_1 to be 18.43°. The constant $\pi\rho\ell$ was set equal to 1, for convenience, as it does not affect the ratio between the random and deterministic variation.

The aformentioned values for velocities and blade angles were used to evaluate the linearization constants F_1, ΔF_i and ΔF_i^*. The results are given in Table 3.

The stator and the rotor blade numbers are kept low, 10 and 20 respectively. It made the calculation easier and from Hodson [HODS 85] having for the turbine 51 rotor blades and 36 stator blades. These values have been used to calculate the linearization constants, as it is done according to the equation (3.15). The subscript k has been dropped because those constants are assumed to be the same from stator to stator. Equation (4.14) was used to evaluate the autocorrelation function of the response due to the deterministic part of the excitation. Here the constant part was dropped since we are not interested in evaluating the part of the response that is constant with time. The autocorrelation of both the deterministic and random part of the response depends on the time difference τ, and time t.

If we set the time difference equal to zero we get the mean square of the response that is a function of t only. Accordingly the mean square of the deterministic part becomes:

$$R_r^D(t) = a^2(\Delta F_i)^2 \sum_{i=1}^{N} \sum_{k=1}^{N} \{\tilde{C}_1 \tilde{C}_1 H_i(\omega_o)H_k^*(-\omega_o)e^{j2\omega_o t} + \tilde{C}_1 \tilde{C}_1^* H_i(\omega_o)H_k^*(\omega_o) + \tilde{C}_1^* \tilde{C}_1 H_i(-\omega_o)H_k^*(-\omega_o)$$

$$+ \tilde{C}_{1_i} {}^{*}\tilde{C}_{1_k} {}^{*}H_i(-\omega_0)H_k{}^{*}(\omega_0)e^{-j2\omega_0 t} \} \quad (5.1)$$

The root mean square (RMS) of the deterministic part obtained from equation (5.1) is plotted in Figure 15. All values given in that figure and the following ones have been normalized with respect to the maximum value of the RMS of the deterministic part. This quantity is a periodic function with frequency equal to two times the frequency of excitation. It appears that the peak of the RMS of the deterministic part occurs between two stator blades.

For the random part, as for the deterministic part, the mean square is found when $\tau = 0$ and then equation (4.17) becomes:

$$R_r^D(t) = (\Delta F_i)^2 \{A(0) + A^*(0) + B(0)e^{j2\omega_0 t} + B^*(0)e^{-j2\omega_0 t}\}$$
$$+ (\Delta F_i^*)^2 \{X(0) + X^*(0) + Y(0)e^{j2\omega_0 t} + Y^*(0)e^{-j2\omega_0 t}\}$$

where

$$A(0) = \frac{1}{2\pi} \sum_{i=1}^{N} \sum_{k=1}^{N} \int_{-\infty}^{+\infty} C_{2_i} C_{2_k}{}^{*} S_{\alpha_i \alpha_k}(\omega_3) \times H_i(\omega_3+\omega_0)H_k{}^{*}(\omega_3+\omega_0)d\omega_3$$

$$B(0) = \frac{1}{2\pi} \sum_{i=1}^{N} \sum_{k=1}^{N} \int_{-\infty}^{+\infty} C_{2_i} C_{2_k}{}^{*} S_{\alpha_i \alpha_k}(\omega_3) \times H_i(\omega_3+\omega_0)H_k{}^{*}(\omega_3-\omega_0)d\omega_3 \quad (5.2)$$

We selected the same spectrum for the parallel inflow velocity represented by α, and the perpendicular velocity denoted by Υ.

Furthermore for simplification comparable parameters are assumed the same. Hence,

$$\sigma_\gamma = \sigma_\alpha$$

$$C_3 = C_1$$

and $C_4 = C_2$

Therefore

$$X(0) = A(0)$$

and $Y(0) = B(0)$

The standard deviation σ_α is a measure of the intensity of turbulence when normalized with respect to the mean inflow velocity $\overline{V_i}$. The intensity of turbulence is defined as a ratio of σ_α to $\bar{V}_i$.

The constants C_1 and C_2 give an idea about the frequency of the turbulence and the scale of the turbulence respectively. Considering the frequency of the turbulence, we observe that it affects only the distribution of energy in various frequencies. More specifically, higher the frequency of turbulence (C_1), higher is the spread of energy in the frequency scale. Indeed the power spectral density function of $\alpha(t)$ and $\gamma(t)$ becomes flatter when the parameter C_1 increases (eq. (4.18)). From the same equation it appears that the correlation of the blade forces does not depend on C_1 and therefore on the frequency of turbulence. The scale of turbulence (C_2), affect both the energy distribution of the driving forces and the statistical correlation between them. The power spectral density function of the excitation becomes flatter and the energy spreads more in the frequency domain, with the scale decreasing. On the other hand, the

correlation between the forces decreases as the scale decreases. This last trend is obvious from the physics of the problem but it can also be deduced from eq. (4.18), where the cross spectral density of $\alpha_i(t)$ and $\alpha_j(t)$ is a monotonically decreasing function with respect to C_2. This trend of the correlation between forces leads to an increase in the magnitude of the response. But the spread of the energy in various frequencies, tends to decrease the response.

In our examples the frequency of the turbulence takes values that are higher than 70 rad/s. The driving frequency is around 448.9 rad/s. Although we do not expect the turbulence frequency to get so low, we evaluated the response for the above range of frequencies to investigate the trend of the blade response with the change of frequency of the turbulence.

The size of the turbulence is selected to be in the range from 1mm to 100 mm. This range of values was selected because the thickness of the boundary layer was estimated and was found to be in the order of 10 mm, Schetz [SCHE 84]. The biggest eddies in a boundary layer of that type can be expected to be in the same range.

In Figure 15, a sample path of the RMS of the response due to random excitation is given. The peaks of this function occur when the blade under consideration is just behind one of the stator blades. For C_1 = 70 rad/s and C_2^{-1} = 50 mm the peak response is about 35%.

In Figure 16, the size of the turbulence is kept constant equal to 50 mm, but the frequency of turbulence is varied from 70 to 30,000 rad/s. Here we observe that by increasing the frequency of turbulence

we flatten the response, i.e. the RMS tends to become constant with time. In Figure 17, the maximum value of the response RMS versus the frequency is plotted. Here we can clearly see that higher frequencies correspond to lower values of the RMS peak. We can also observe that if we decrease the size of the turbulence the response also decreases. In Figure 18 we have the same plot but higher values for the response on the peak because the turbulence intensity is higher.

Finally in Figures 19 and 20 the peak of the response due to random excitation is plotted as a function of the size of the turbulence. We observe that the response increases with increasing size of turbulence. Again higher frequencies of turbulence correspond to lower response levels.

Chapter 6 Conclusions and Recommendations for Future Work

6.1 Conclusions

The results of this research show that the variability in the exciting forces may lead to a significant increase in the vibratory response and therefore the chance of a catastrophic failure. Furthermore, it may decrease the expected life of the assembly. Consequently, it is important to consider the random part of the blade forces in analyzing the reliability of the blades.

The example studied resulted in amplitude of the RMS for the random part as high as 35% of the deterministic part. This is a significant effect and should not be overlooked. Such a high value increases the probability of a first excursion failure of the blades. For higher frequencies of turbulence the amplitude of the RMS decreases. But the number of cycles that the blade-disk assembly goes through, increases with higher frequency. Therefore the probability of a fatigue failure will increase with higher frequency of turbulence.

It is important to realize what happens when the frequency of turbulence and the frequency of excitation (which is the first natural frequency in this case) are close to each other. When this happens, it appears that the amplitude reaches its maximum. In our case, we had a slow turning turbine and therefore the frequency of the turbulence had to be very low to coincide with the excitation frequency. In most cases, turbines turn very fast in the range 10,000 to 40,000 rpm. In such a case, it is very likely that the two

aformentioned frequencies are close. The size of the eddies on the scale of turbulence is also important. Larger eddies result in an increased correlation between the blades. This in turn will lead to a higher response. The previous conclusions are summarized as follows:

1) Low frequencies and/or large scale of turbulence will lead to a high amplitude of the RMS of the random part. This will increase the likelihood of a first excursion failure.
2) High frequencies of turbulence will lower the amplitude of the RMS. But however, higher frequencies will increase the probability of a fatigue failure.
3) When the frequency of turbulence and the frequency of the excitation coincide, we have a high response.

6.2 Recommendations for Future Work

Certain limitations of the present research: Firstly, only one harmonic of the excitation is studied, but however, we account for many harmonics in the transfer functions. Secondly, we formulate only the forces in one-dimension when they are actually three-dimensional. This is the most difficult task to fulfill. The flowfield in a stator/rotor combination is one of the most complex encountered, therefore, it is difficult to model the forces accurately. In the present research, a slow turning turbine was used as an example. Most turbines turn very fast and are very compact. Therefore we recommend that such a turbine will be studied in future research.

The force on the blades is a amplitude modulated signal (AM process). Therefore we have two frequencies, the amplitude modulation frequency and the carrier frequency. From eq. (5.2) we can see that when the difference and the summation of the two frequencies coincide with one of the natural frequencies of the structure we should get a very high response.

Consideration should be given to statistical energy analysis of this problem or using an amplitude modulated white noise. Finally we recommend that first excursion failures and fatigue failure be studied. It would be worthwhile to study such effects in line with mistuning of the bladed-disk assembly i.e. when the blades do not all have the same natural frequencies.

References

[BLAKE 70] Blake, W.K., "Turbulent Boundary-Layer Wall Pressure Fluctuations on Smooth and Rough Walls," Journal of Fluid Mechanics, (1970), Vol. 44, part 4, pp. 653-660.

[CRAIG 81] Craig, R.R. Jr., Structural Dynamics, John Wiley and Sons, Inc., 1981.

[EWIN 76] Ewins, D.J. and Sadasiva Rao, Y.V.K., "A Theoretical Study of the Damped Forced Vibration Response of Bladed Discs," Structural Dynamic Aspects of Bladed Disk Assemblies, The Winter Annual Meeting of ASME, NY, 1976, pp. 29-43.

[EWIN 80] Ewins, D.J., "Bladed Disc Vibration - A Review of Techniques and Characteristics," Proceedings of International Conference on Recent Advances in Structural Dynamics, Southampton, 1980, pp. 187-210.

[EWIN 83] Ewins, D.J. and Srinivasan, A.V. (Eds.), "Vibration of Bladed Disk Assemblies," ASME 1983, Vibrations Conference.

[FRAN 69] Franks, L., Signal Theory, Englewood Cliffs, NJ: Prentice Hall, 1969.

[GARD 75] Gardner, W.A. and Franks, L.E., "Characterization of Cyclostationary Random Signal Processes," IEEE Transaction on Information Theory, Vol. IT-21, No. 1, January 1975, pp. 4-14.

[GLAD 63] Gladyshev, E.G., "Periodically and Almost Periodically Correlated Random Processes with Continuous Time Parameter," Theory Prob. Appl. (USSR), pp. 173-177, 1963.

[GRIF 84] Griffin, J.H. and Hoosac, T.M., "Model Development and Statistical Investigation of Turbine Blade Mistuning," Journal of Vibration, Acoustics, Stress, and Reliability in Design, Vol. 106, April 1984, pp. 204-210.

[GUDZ 59] Gudzenko, L.I., "On Periodic Nonstationary Processes," Radio Eng. Electron. Phys. (USSR), Vol. 4, No. 6, pp. 220-224, 1959.

[HODS 72] Hodson, H.P., "The Development of Unsteady Boundary Layers on the Rotor of an Axial Flow Turbine," AGARD-CP-351, Copenhagen, June 1983.

[HODS 85] Hodson, H.P., "Measurements of Wake-Generated Unsteadiness in the Rotor Passages of Axial Flow Turbines," ASME, Journal of Engineering for Gas Turbines and Power, Vol. 107, April 1985, pp. 467-474.

[HURD 69] Hurd, H., "An Investigation of Periodically Correlated Stochastic Processes," Ph.D. Dissertation, Duke Unviersity, Durham, NC, 1969.

[IRRE 84] Irretier, H., "Numerical Analysis of Transient Responses in Blade Dynamics," Third International Conference on Vibrations in Rotating Machinery, The Institution of Mechanical Engineers, NY, 1984.

[JAY 84] Jay, R.L., MacBain, J.G. and Burns, D.W., "Structural Response Due to Blade Vane Interaction," ASME, Journal of Engineering for Gas Turbines and Power, Vol. 106, January 1984, pp. 50-56.

[KARAM 66] Karamcheti, K., Principles of Ideal-Fluid Aerodynamcis, Robert E. Krieger Publishing Corp., Malabar, FL, 1966.

[KERR 77] Kerrebrock, J.L., Aircraft Engines and Gas Turbines, The Massachusetts Institute of Technology, 1977.

[LEIS 81] Leissa, A.W., "Vibrational Aspects of Rotating Turbomachinery Blades," Applied Mechanics Reviews, Vol. 34, No. 5, 1981, pp. 629-635.

[LEIS 84] Leissa, A.W., et al., "Vibrations of Twisted Cantilevered Plates - Summary of Previous and Current Studies," Journal of Sound and Vibration.

[MCGR 87] McGrath, B.E. and Simpson, R.L., "Some Features of Surface Pressure Fluctuations in Turbulent Boundary Layers with Zero and Favorable Pressure Gradients," Virginia Polytechnic Inst. and State Univ., NASA Contractor Report 4051, Langley Research Center, 1987.

[NIKO 85a] Nikolaidis, E., "Structural Reliability of Marine Diesel Engine Propulsion Shafting Systems," Ph.D. Thesis, Department of Naval Architecture and Marine Engineering, The University of Michigan, 1985.

[NIKO 85b] Nikolaidis, E., Perakis, A.N. and Parsons, M.G., "Structural Reliability of Marine Diesel Engine Propulsion Shafting Systems," SNAME Transactions, Vol. 93, 1985, pp. 189-223.

[NIKO 87] Nikolaidis, E., Perakis, A.N. and Parsons, M.G., "Probabilistic Torsional Vibration Analysis of a Motor Ship Propulsion Shafting System: The Input-Output Problem," Journal of Ship Research, Vol. 31, No. 1, March 1987, pp. 41-52.

[OATES 84] Oates, G.C., "Aerothermodynamics of Gas Turbine and Rocket Propulsion," American Institute of Aeronautics and Astronautics, Inc., New York, NY, 1984.

[OGUR 71] Ogura, H., "Spectral Representation of a Periodic Nonstationary Random Process," IEEE Transactions on Information Theory, Vol. IT-17, pp. 143-149, March 1971.

[PANT 74] Panton, R.L. and Linebarger, J.H., "Wall Pressure Spectra Calculations for Equilibrium Boundary Layers," Journal of Fluid Mechanics, (1974), Vol. 65, part 2, pp. 261-287.

[PAPO 83] Papoulis, A., "Random Modulation: A Review," IEEE Transactions on Acoustic, Speech and Signal Processing, Vol. ASSP-31, No. 1, pp. 96-105, February 1983.

[RAO 80] Rao, J.S., "Turbomachine Blade Vibration," Shock and Vibration Digest, Vol. 12, 1980, pp. 19-26.

[RAO 83] Rao, J.S. and Jadvani, H.M., "Free and Forced Vibrations of Turbine Blades," Proceedings, Vibrations of Bladed Disk Assemblies, 9th ASME Conference in Mechanical Vibrations and Noise, Dearborn, MI, 1983, pp. 11-24.

[SCHE 84] Schetz, J.A., Foundations of Boundary Layer Theory, Prentice-Hall, Inc., Englewood Cliffs, NJ, 1984.

[SCHL 79] Schlichting, H., Boundary Layer Theory, Seventh Edition, McGraw Hill, NY, 1979.

[SRIN 78] Srinivasan, A.V., Lionberger, S.R. and Brown, K.W., "Dynamic Analysis of an Assembly of Shrouded Blades using Component Modes," ASME Journal of Mechanical Design, Vol. 100, 1978, pp. 520-527.

[TOWNS 76] Townsend, A.A., The Structure of Turbulent Shear Flow, Cambridge Univ. Press, 1976.

[Walker 72] Walker, G.J. and Oliver, A.R., "The Effect of Interaction Between Wakes from Blade Rows in an Axial Flow Compressor on the Noise Generated by Blade Interaction," ASME, Journal of Engineering for Power, October 1972, pp. 241-248.

Tables

Table 1: Values of Model Parameters

m_1 = 0.0541 kg

m_2 = 0.0299 kg

K_1 = 419,886 N/m

K_2 = 7,521,000 N/m

K_6 = 30,840,000 N/m

C = 0.6907 s•N/m

Table 2: Sensitivity of the Model to Variations in the Applied Forces

Case No.	C.O.V. Forces $\frac{\sigma_F}{\mu_F}$	C.O.V. Displacement $\frac{\sigma_X}{\mu_X}$	Max Displacement/ Equal Displacement $\frac{X_{max}}{X_{eq}}$
1	.0003	.0297	1.073
2	.0032	.2892	1.735
3	.1239	.4762	19.364
4	.1627	.4707	22.448

Table 3: Test Case Data

ω_o = 448.908 rad/s

N = 20 rotor blades

S = 10 stator blades

$\overline{V_i}$ = 300 m/s

$\overline{V_i^*}$ = 0 m/s

(ωr) = 330 m/s

α_1 = 0°

θ_1 = 60°

β_1 = 18.43°

β = 5°

$\pi\rho\ell$ = 1 kg/m^2

F_1 = 2394.35 N

ΔF_i = 167.48 $\frac{N}{m/s}$

ΔF_i^* = 14.60 $\frac{N}{m/s}$

Figures

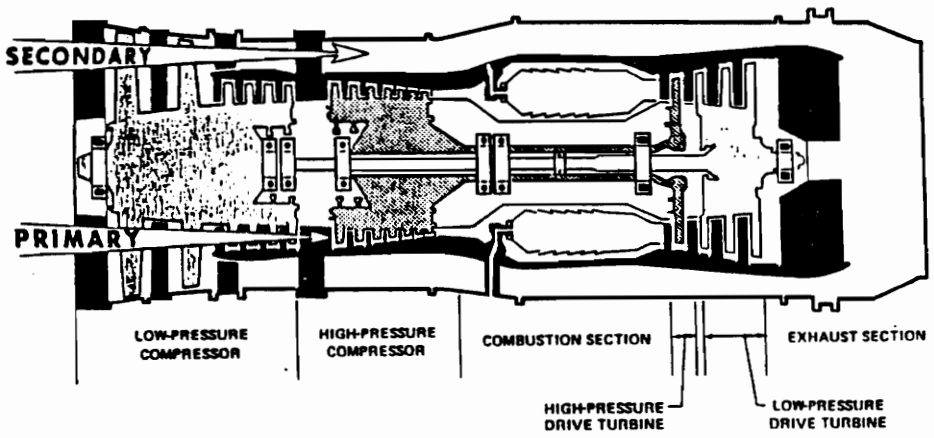

Figure 1 Turbofan Engine

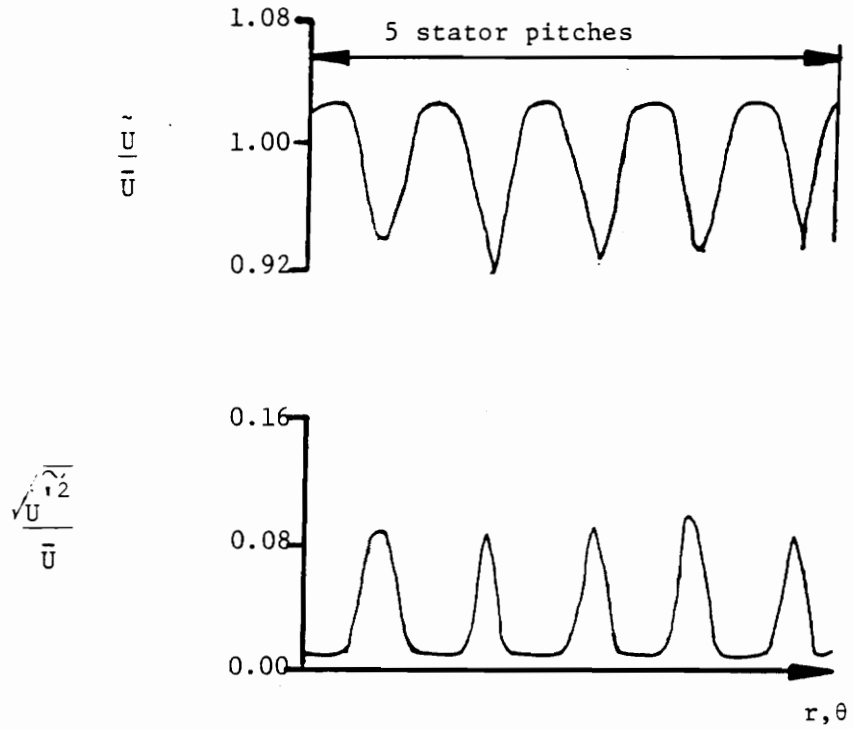

Figure 2 Ensembled Root Mean Square, and Ensembled Mean of Instantaneous Flow Velocity, [HODS 85]

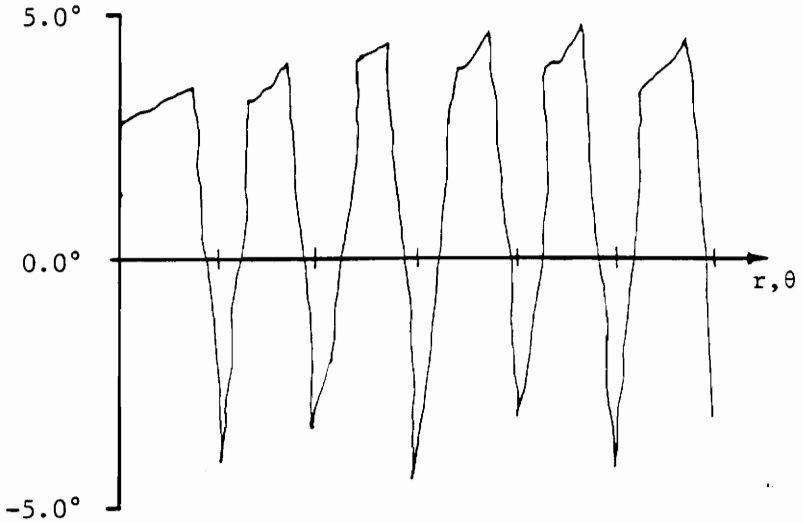

Figure 3 Incidence Angle [HODS 85]

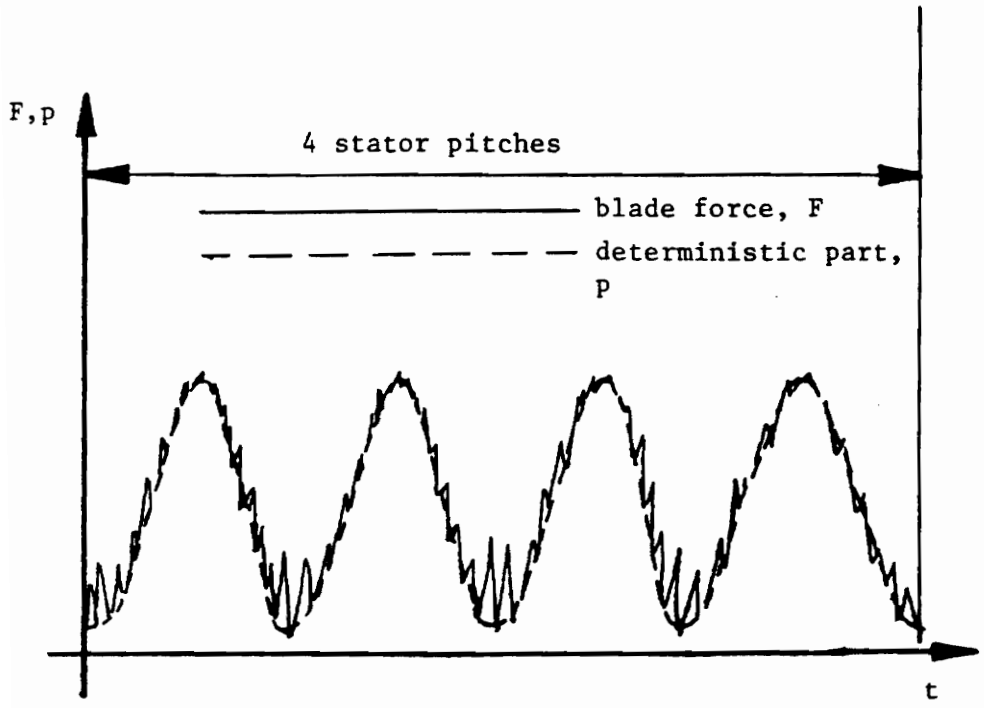

Figure 4 Sample Path of Blade Force

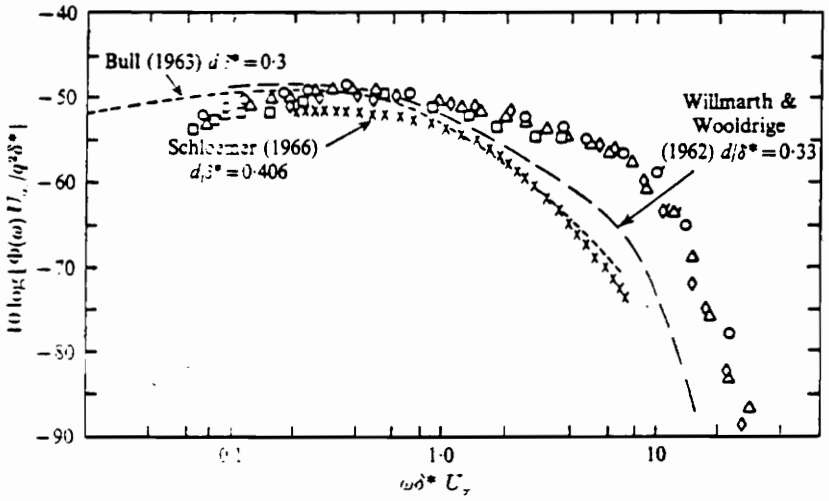

Figure 5 Smooth-Wall Pressure Spectrum [BLAKE 70]

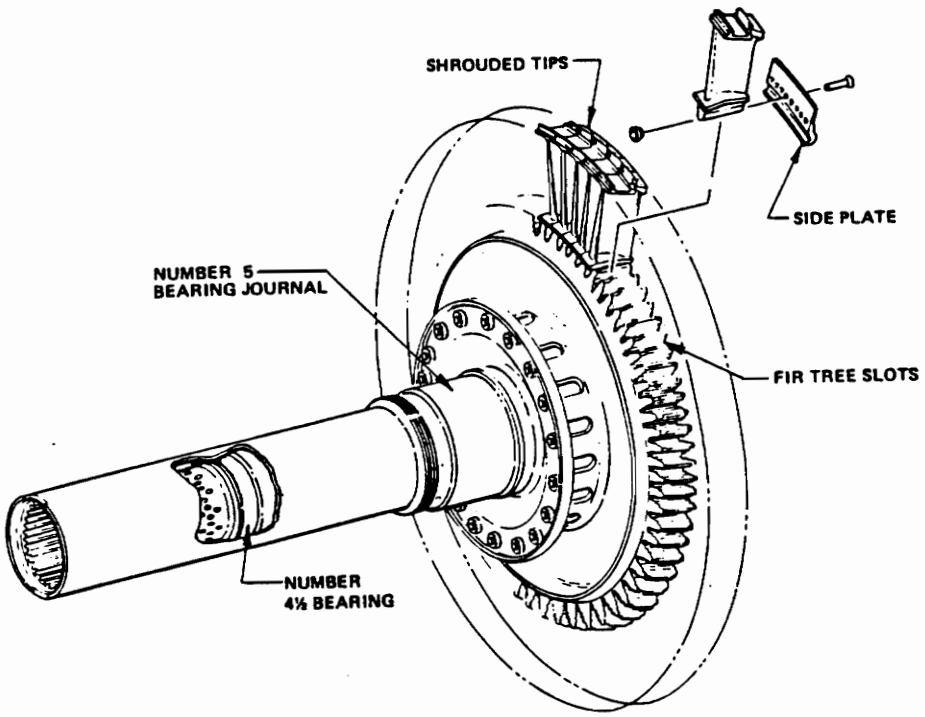

Figure 6 Bladed-Disk Assembly Layout

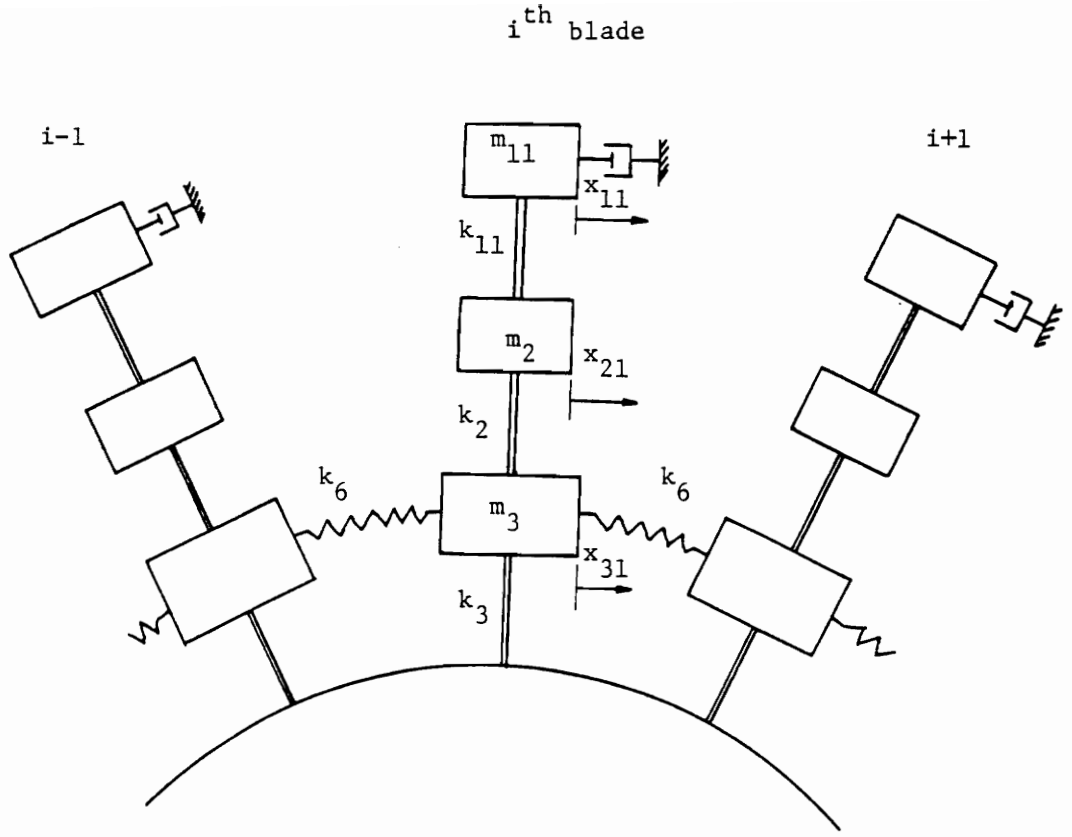

Figure 7 3-DOF Model of a Bladed-Disk Assembly

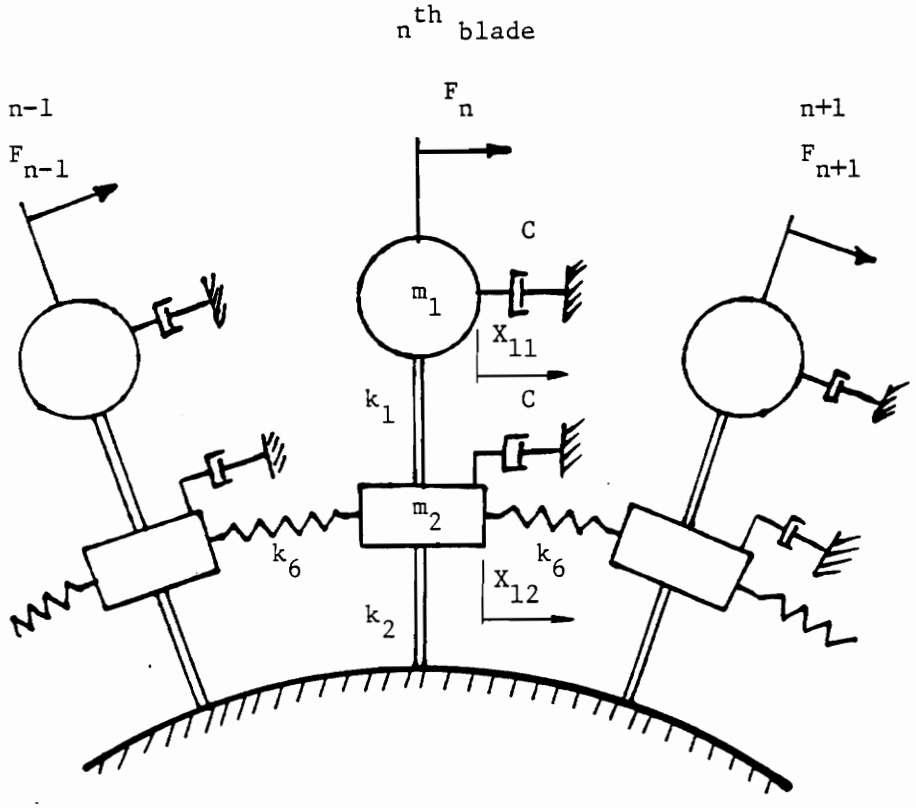

Figure 8 2-DOF of a Bladed-Disk Assembly

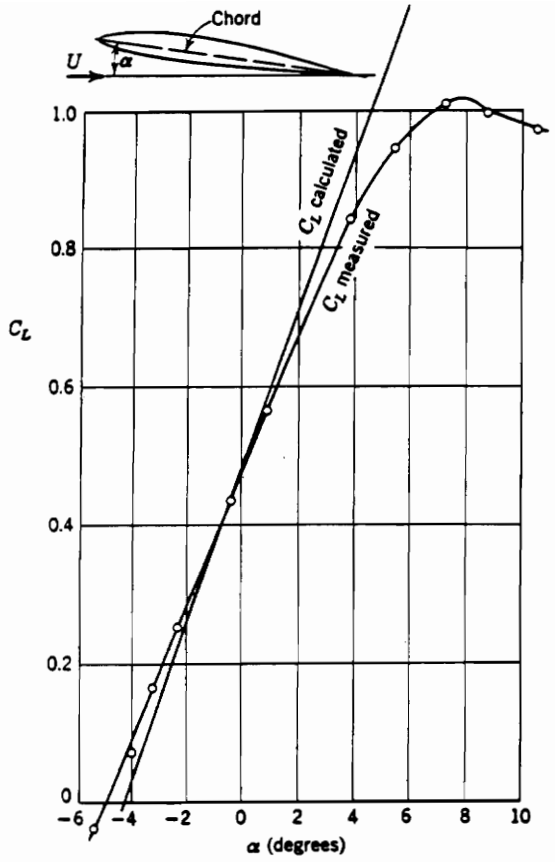

Figure 9 Comparison of a Theoretical and Experimental Results for the Lift of an Airfoil [KARAM 66]

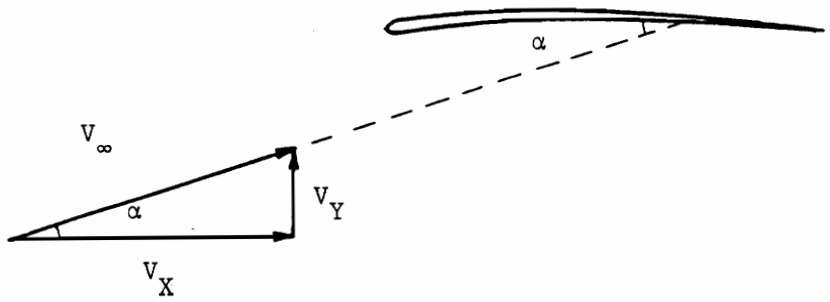

Figure 10 Dependence of α on V_X and V_Y

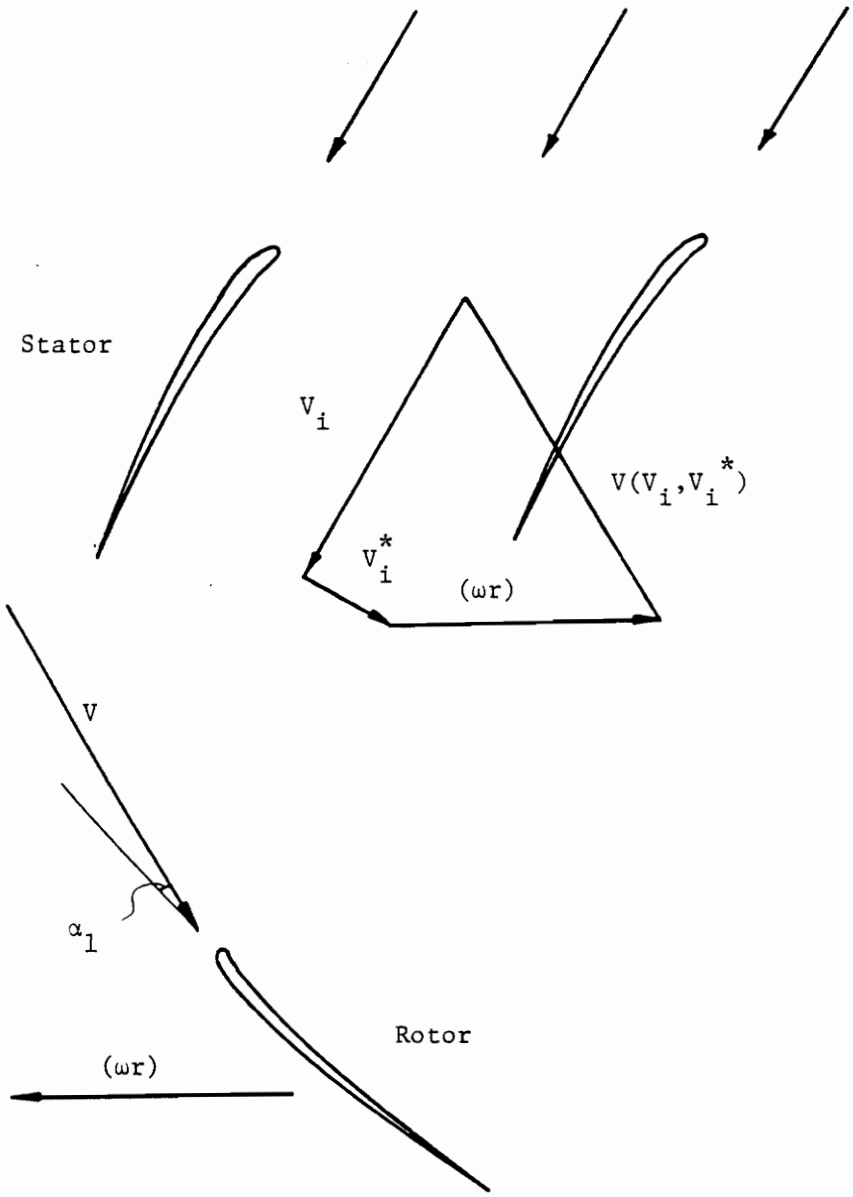

Figure 11 Velocity Triangles

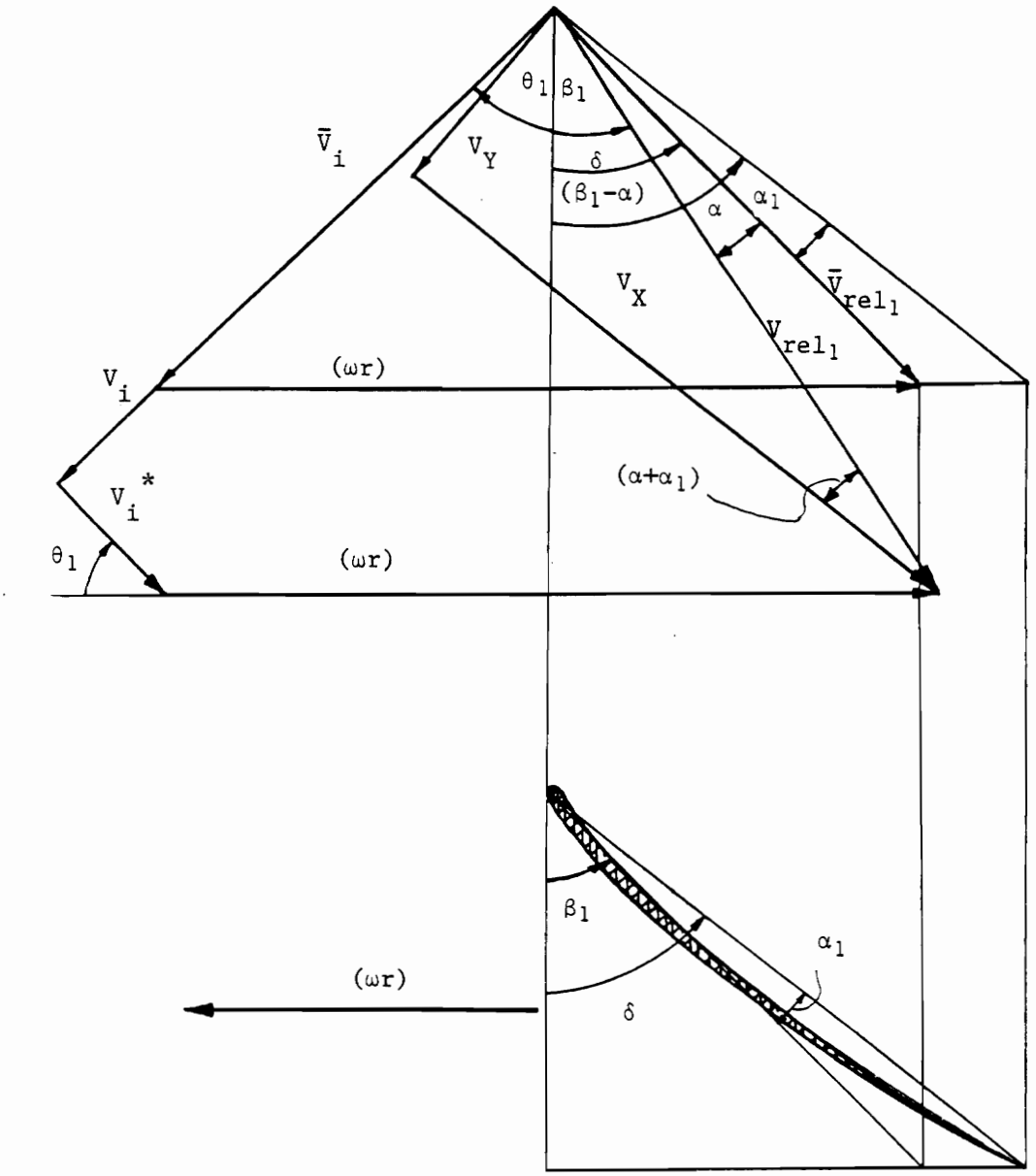

Figure 12 Inflow Velocity Diagrams

$t_2 = t$

$t_1 = t + \tau$

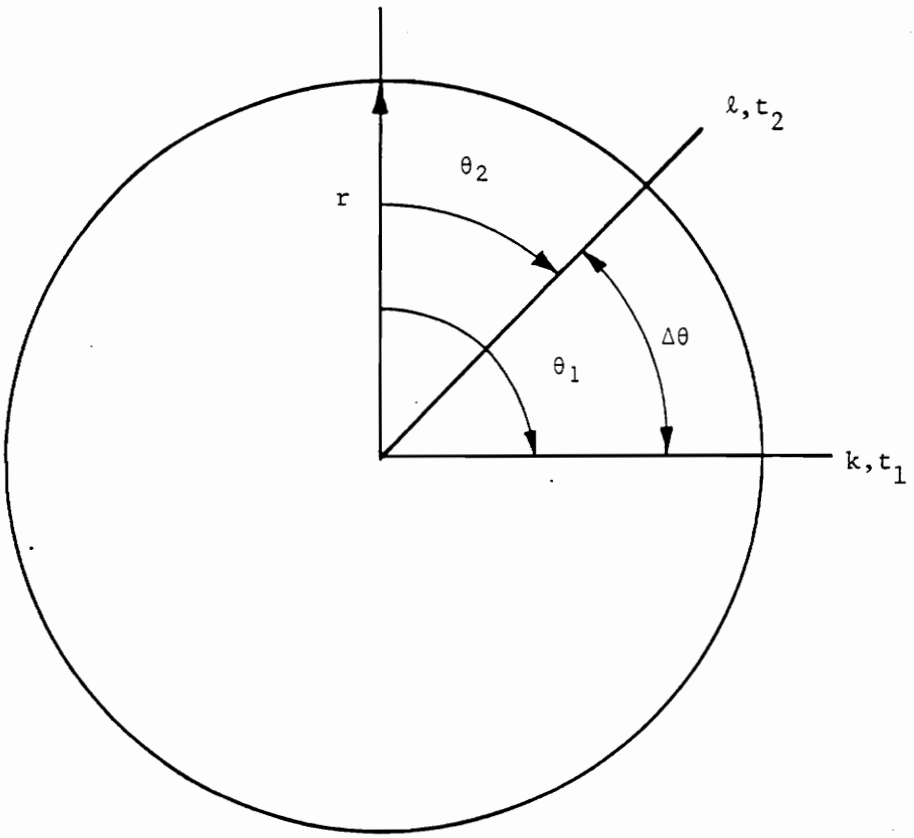

Figure 13 Fixed Coordinate System
Blade ℓ at time t_2 and blade
k at time t_1

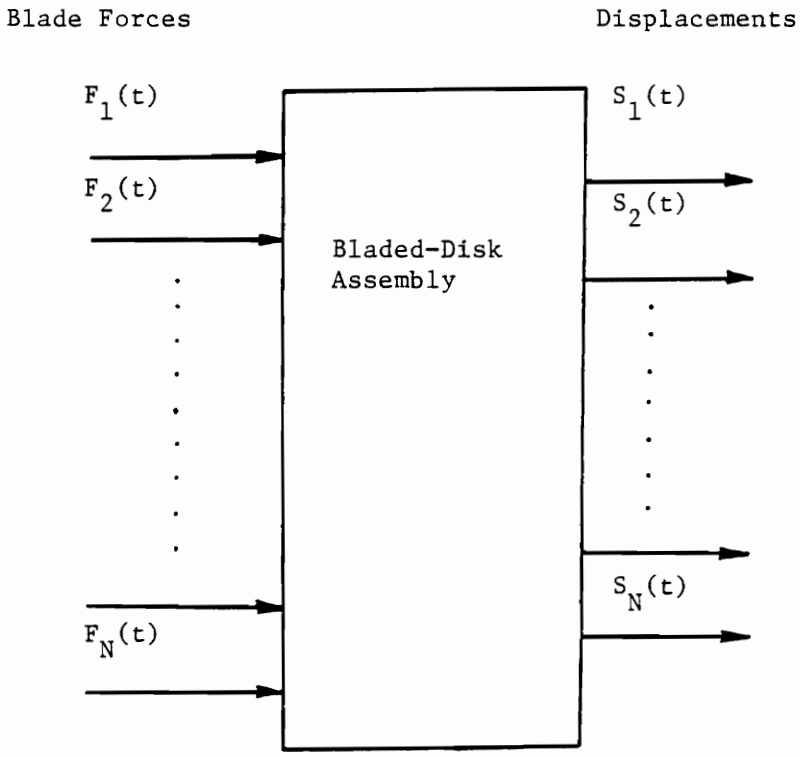

Figure 14 The System with the Inputs and the Outputs

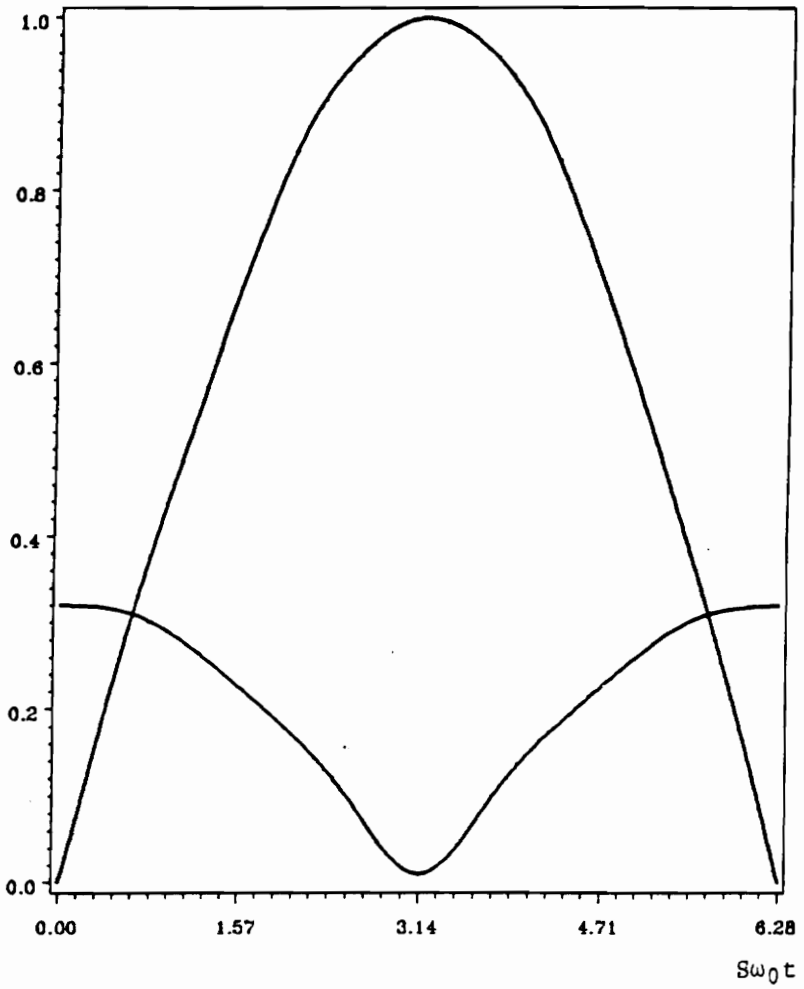

Figure 15 Sample Path of Random and Deterministic Variation

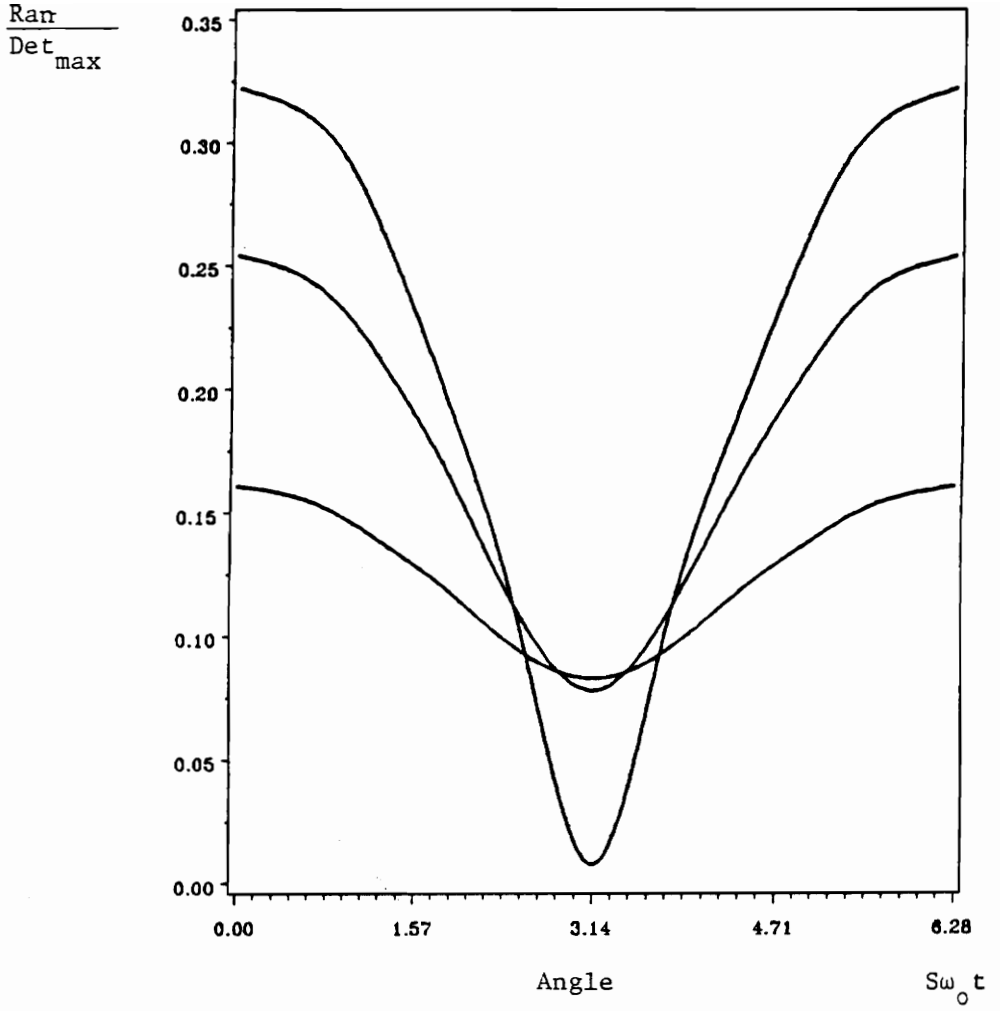

Figure 16 Sample Path of a Random Variation

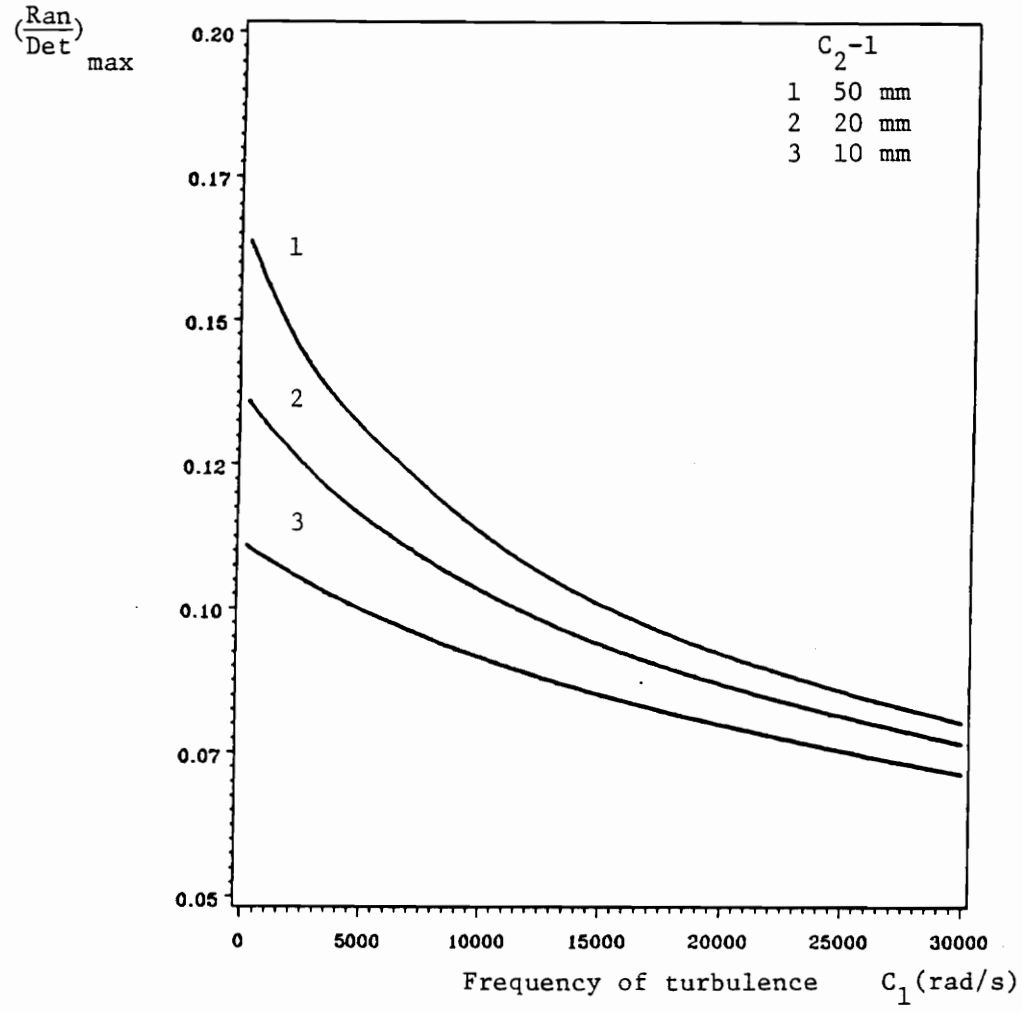

Figure 17 Comparison, Random and Deterministic Variation as a Function of C_1.

$\sigma_\alpha/\bar{V}_i$ = 5%, $a/\bar{V}_i$ = 5%.

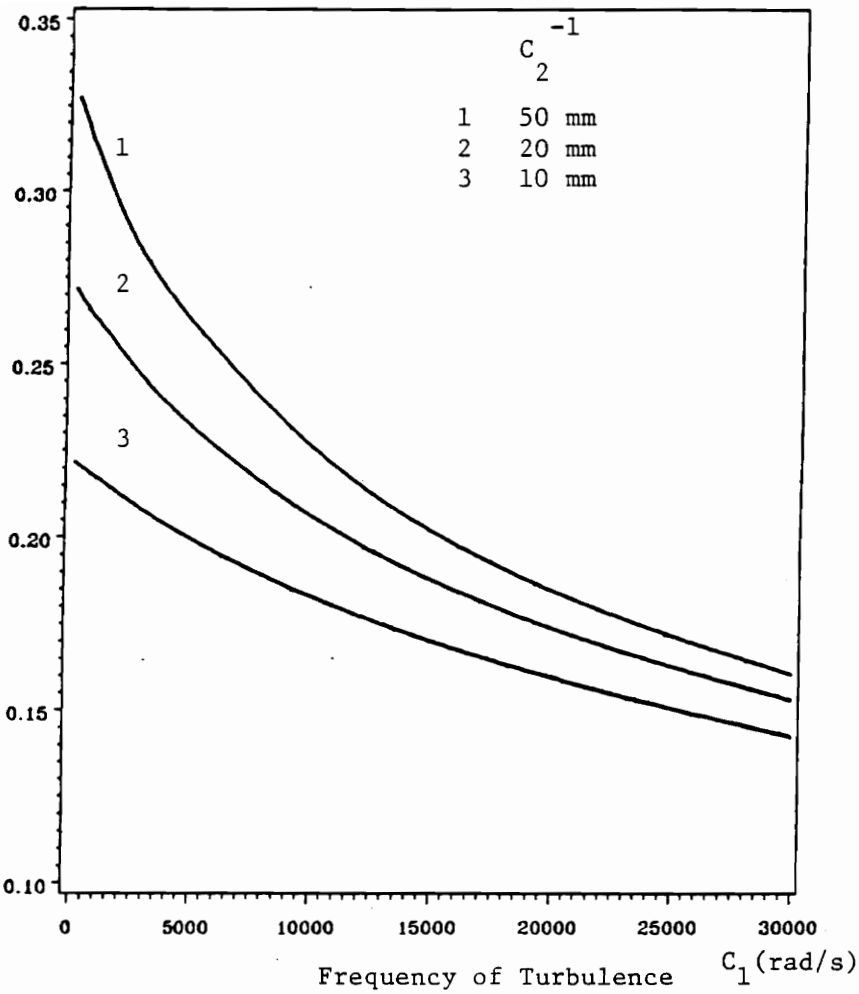

Figure 18 Comparison, Random and Deterministic Variation as a Function of C_1.

$\sigma_\alpha/\bar{V}_i$ = 10%, $a/\bar{V}_i$ = 5%

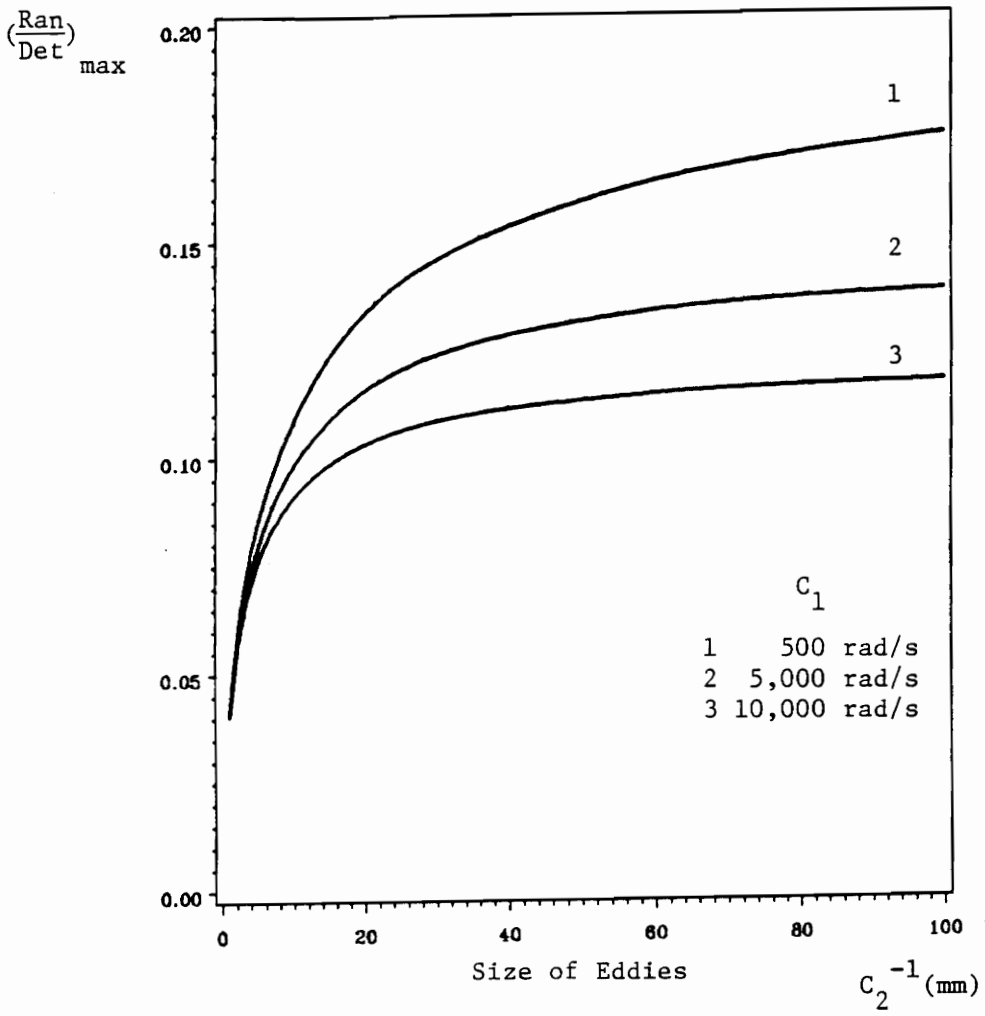

Figure 19 Comparison, Random and Deterministic Variation as a Function of C_2^{-1}.

$\sigma_\alpha/\bar{V}_i$ = 5%, $a/\bar{V}_i$ = 5%

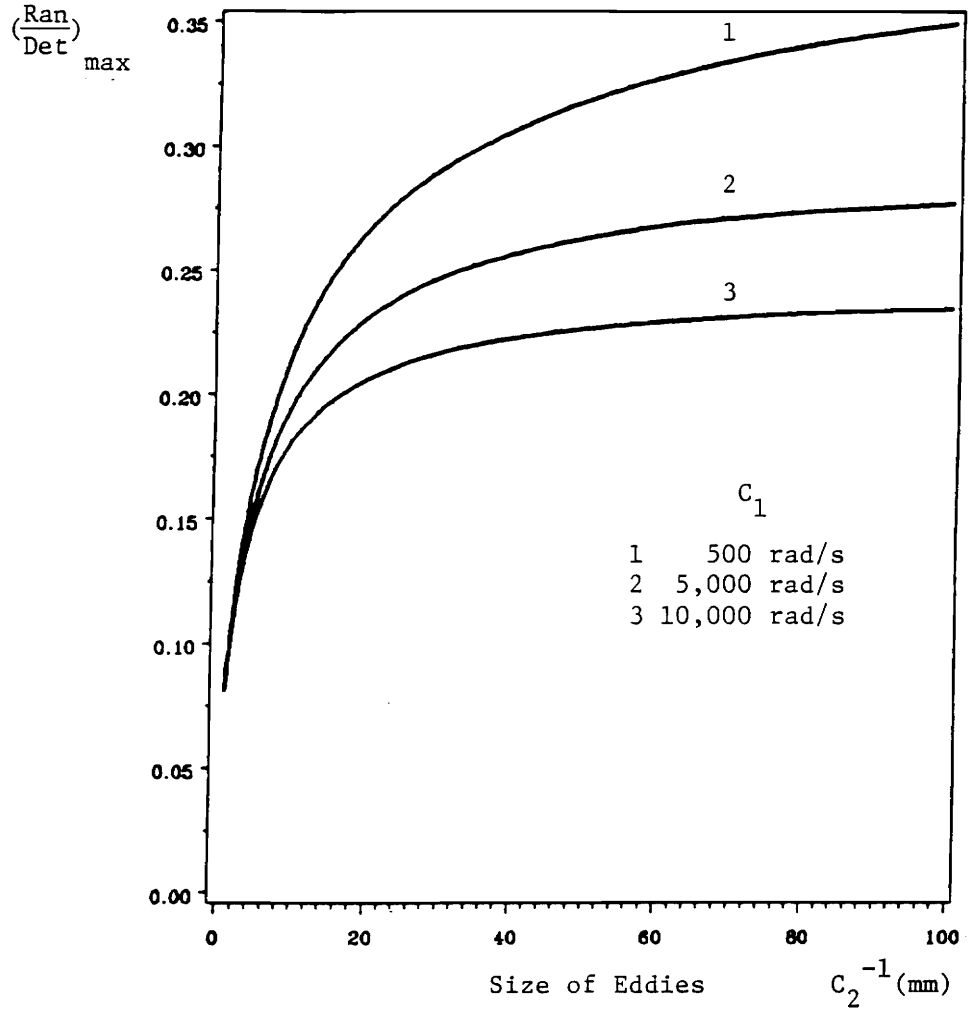

Figure 20 Comparison, Random and Deterministic Variation as a Function of C_2^{-1}.

$\sigma_\alpha/\bar{V}_i = 10\%$, $a/\bar{V}_i = 5\%$

APPENDIX

The statistical properties of the output of a multi-input time invariant linear system will be derived.

The double Fourier transform of $R(t+\tau,t)$ with respect to t and τ is defined as follows:

$$\Delta(\omega_1,\omega_2) = \int_{-\infty}^{+\infty}\int_{-\infty}^{+\infty} R(t+\tau,t)e^{-j(\omega_1\tau-\omega_2 t)}\,d\tau dt \qquad (A\text{-}1)$$

hence

$$R(t+\tau,t) = \frac{1}{(2\pi)^2}\int_{-\infty}^{+\infty}\int_{-\infty}^{+\infty} \Delta(\omega_1,\omega_2)e^{j(\omega_1\tau-\omega_2 t)}\,d\omega_1 d\omega_2 \qquad (A\text{-}2)$$

In the same way the double Fourier transform of $R(t_1,t_2)$ is defined as:

$$\Gamma(\omega_1,\omega_2) = \int_{-\infty}^{+\infty}\int_{-\infty}^{+\infty} R(t_1,t_2)e^{-j(\omega_1 t_1-\omega_2 t_2)}\,dt_1 dt_2 \qquad (A\text{-}3)$$

inversion formula

$$R(t_1,t_2) = \frac{1}{(2\pi)^2}\int_{-\infty}^{+\infty}\int_{-\infty}^{+\infty} \Gamma(\omega_1,\omega_2)e^{j(\omega_1 t_1-\omega_2 t_2)}\,d\omega_1 d\omega_2 \qquad (A\text{-}4)$$

The relationship between $\Delta(\omega_1,\omega_2)$ and $\Gamma(\omega_1,\omega_2)$ is as follows:

$$\Delta(\omega_1,\omega_2) = \Gamma(\omega_1,\omega_1+\omega_2) \qquad (A\text{-}5)$$

Proof.

From (A-3) we have, with

$$t_1 = t+\tau \qquad t_2 = t$$

$$\Gamma(\omega_1,\omega_2) = \int_{-\infty}^{+\infty}\int_{-\infty}^{+\infty} R(t+\tau,t)e^{-j(\omega_1\tau-(\omega_2-\omega_1)t)}\,d\tau dt$$

hence, adding ω_1 to ω_2 we obtain

$$\Gamma(\omega_1,\omega_1+\omega_2) = \int_{-\infty}^{+\infty}\int_{-\infty}^{+\infty} R(t+\tau,t)e^{-j(\omega_1\tau-\omega_2 t)}\,d\tau dt \qquad (A\text{-}6)$$

This integral is the definition of $\Delta(\omega_1,\omega_2)$ and therefore the relationship given by (A-5) is proven. This relationship will be used in the next derivation.

Next we want to show that the double Fourier transform of the autocorrelation of the output $r(t)$ of an N-input time-invariant linear system with respect to t and τ is given by equation (4.7):

$$\Delta_r(\omega_1,\omega_2) = \sum_{i=1}^{N}\sum_{k=1}^{N} \Delta_{s_j s_k}(\omega_1,\omega_2)H_i(\omega_1)H_k^*(\omega_1+\omega_2)$$

Proof.

For a linear system with inputs $s_i(t)$ and $s_k(t)$ the autocorrelation of the output $r(t)$ is given by:

$$R_{r_\ell}(t_1,t_2) = \sum_{i=1}^{N}\sum_{k=1}^{N} R_{s_i s_k}(t_1,t_2)h_{\ell,i}(t_1)h_{\ell,k}^*(t_2) \qquad (A\text{-}7)$$

The index ℓ is for blade number ℓ, but because all the blades have the same autocorrelation it is dropped later. The $h_{\ell,i}(t_1)$ and $r_{\ell,k}^*(t_2)$ are the elements of a impulse response matrix for the multi-input, multi-output system. The transfer matrix in this case becomes an Nx1 vector with elements $H_i(\omega)$, i=1,...,N. Taking the double Fourier transform of $R_r(t_1,t_2)$(ℓ has been dropped) we have, with

$$t_1 = t + \tau \qquad t_2 = t$$

$$\Gamma_r(\omega_1,\omega_1+\omega_2) = \sum_{i=1}^{N}\sum_{k=1}^{N} \int_{-\infty}^{+\infty}\int_{-\infty}^{+\infty} R_{s_i s_k}(t+\tau,t)h_i (t+\tau)h_k^*(t)e^{-j(\omega_1,\tau-\omega_2 t)} d\tau dt$$

$$= \sum_{i=1}^{N}\sum_{k=1}^{N} \Gamma_{s_i s_k}(\omega_1,\omega_1+\omega_2)H_i(\omega_1)H_k^*(\omega_1+\omega_2) \qquad \text{(A-8)}$$

Finally by replacing $\Gamma(\omega_1,\omega_1+\omega_2)$ with $\Delta(\omega_1,\omega_2)$ as shown in (A-5), we have

$$\Delta_r(\omega_1,\omega_2) = \sum_{i=1}^{N}\sum_{k=1}^{N} \Delta_{s_i s_k}(\omega_1,\omega_2)H_i(\omega_1)H_k^*(\omega_1+\omega_2)$$

Equation (4.7) is thereby derived.

Vita

The author was born in Reykavik, Iceland on April 8, 1962. He entered the University of Iceland, Reykavik in 1982. He graduated in June 1986 with a degree in Mechanical Engineering. He began his studies at Virginia Polytechnic Institute and State University in September 1986 to pursue graduate study in Aerospace Engineering. He is to be awarded a Master of Science in Aerospace Engineering in June 1988.

Sveinn V. Ólafsson.